Subcellular mRNA localization regulates ribosome biogenesis in migrating cells

Maria Dermit[1], Martin Dodel[1], Flora C. Y. Lee[2,3], Muhammad S. Azman[1], Hagen Schwenzer[4], J. Louise Jones[5], Sarah P. Blagden[4], Jernej Ule[2,3], & Faraz K. Mardakheh[1*].

1: *Centre for Cancer Cell and Molecular Biology, Barts Cancer Institute, Queen Mary University of London, Charterhouse square, London EC1M 6BQ, United Kingdom.*
2: *The Francis Crick Institute, 1 Midland Road, London NW1 1AT, United Kingdom.*
3: *Department of Neuromuscular Diseases, UCL Queen Square Institute of Neurology, Queen Square, London WC1N 3BG, United Kingdom.*
4: *Department of Oncology, University of Oxford, Oxford OX3 7DQ, United Kingdom.*
5: *Centre for Tumour Biology, Barts Cancer Institute, Queen Mary University of London, Charterhouse square, London EC1M 6BQ, United Kingdom.*
***:** *Correspondence: f.mardakheh@qmul.ac.uk*

Summary

Translation of Ribosomal Protein coding mRNAs (RP-mRNAs) constitutes a key step in regulation of ribosome biogenesis, but the mechanisms which modulate RP-mRNAs translation under various cellular and environmental conditions are poorly understood. Here we show that the subcellular localization of RP-mRNAs acts as a key regulator of their translation in migrating cells. As cells migrate into their surroundings, RP-mRNAs localize to the actin-rich protrusions at the front the cells. This localization is mediated by La related protein-6 (LARP6), an RNA Binding Protein that is enriched in protrusions. Protrusions act as hotspots of translation for localized RP-mRNAs, resulting in enhancement of RP synthesis, up-regulation of ribosome biogenesis, and increased overall protein synthesis of migrating cells in a LARP6 dependent manner. In human breast carcinomas, Epithelial to Mesenchymal Transition (EMT) upregulates LARP6 expression to enhance protein synthesis, and can be targeted using a small molecule inhibitor that interferes with LARP6 RNA binding. Our findings reveal LARP6 mediated mRNA localization as a key regulator of ribosome biogenesis during cell-migration, and demonstrate a role for this process in cancer progression downstream of EMT.

Introduction

Ribosome biogenesis, the highly conserved process of synthesis, modification, and assembly of ribosomal RNA (rRNA) and protein (RP) components into mature ribosomal subunits, is elevated in nearly all human cancers (Ruggero and Pandolfi, 2003). This upregulation is critical for boosting protein synthesis, in order to maintain the increased anabolic demands of malignant cells (Pelletier et al., 2018). Enhanced protein synthesis is particularly important for supporting invasion and metastasis in high-grade cancers (Hsieh et al., 2012; Mendillo et al., 2012), although the mechanisms that allow invasive cancer cells to augment their ribosome biogenesis remain poorly understood. Crucially, regulation of rRNAs and RPs synthesis is largely uncoupled in higher eukaryotes (Granneman and Tollervey, 2007), with translation of RP-mRNAs acting as the key step in control of RP levels and ribosome biogenesis (Hsieh et al., 2012; Thoreen et al., 2012).

It is now clear that rather than being uniformly distributed throughout the cytoplasm, the majority of eukaryotic mRNAs exhibit specific subcellular localizations (Benoit Bouvrette et al., 2018; Lecuyer et al., 2007; Wang et al., 2012; Wilk et al., 2016). Such localization can act as a means of localizing the encoded proteins (Zappulo et al., 2017), or function instead as a mechanism for post-transcriptional regulation by modulating the access of mRNAs to different *trans*-acting factors (Kejiou and Palazzo, 2017; Pizzinga et al., 2019; Prasanth et al., 2005). Interestingly, several studies have reported that RP-mRNAs can localize to various forms of cellular projections such as actin-rich protrusions at the front of mesenchymal-like migratory cells or axons of neurons (Andreassi et al., 2010; Briese et al., 2016; Gumy et al., 2011; Mardakheh et al., 2015; Mili et al., 2008; Saal et al., 2014; Shigeoka et al., 2016; Taylor et al., 2009; Wang et al., 2017; Zivraj et al., 2010). Nevertheless, the molecular mechanism and functional significance of RP-mRNAs localization has remained unclear.

Here we employed a subcellular multi-omics analysis to demonstrate that RP-mRNA localization to actin-rich protrusions is a universal feature of migratory cells. This localization is mediated via LARP6, a microtubule-associated RNA Binding Protein (RBP) that binds to RP-mRNAs to promote their enrichment in protrusions. Protrusions are also highly enriched in translation initiation and elongation factors, acting as hotspots for translation of localized RP-mRNAs. LARP6 dependent localization of RP-mRNAs results in upregulation of RP levels, leading to enhancement of ribosome biogenesis and global protein synthesis in migrating cells. In human breast carcinomas, higher LARP6 protein expression is associated with the invasive mesenchymal-like subtypes. EMT induces LARP6 protein expression, which acts to promote malignant growth and invasion. Crucially, LARP6 regulation of RP-mRNAs can be therapeutically targeted using small molecule inhibitors which specifically interfere with its RNA binding. Collectively, our findings reveal a new mechanism that governs ribosome biogenesis in mesenchymal-like migratory cells via subcellular localization of RP-mRNAs, and demonstrate a therapeutically targetable role for this process in cancer downstream of EMT.

Results

RP-mRNAs localize to protrusions of all migratory cells

We utilized a micro-porous transwell filter based method (Mardakheh et al., 2015; Mili et al., 2008) to assess if RP-mRNAs localization to actin-rich protrusions was a conserved feature of all migratory cells. We modified the procedure to allow cells to adhere to the top of the filter first, followed by synchronized induction of protrusion formation through the pores (Figure 1A). Importantly, the small (3μm) size of the pores enables protrusions to form but prevents the cell bodies from passing through, thus resulting in separation of the protrusions and the cell bodies on opposite sides of the filter, which can be independently imaged or purified for multi-omics analysis (Figure 1A). Using this method, we profiled the subcellular distribution of mRNAs in a diverse panel of normal and malignant migratory cell-lines from various cell-types and tissues of origin (Figure 1B). RNA-seq analysis of protrusion and cell-body fractions revealed RP-mRNAs to be enriched in protrusions of all cell-lines (Figure 1C & Dataset S1), strongly supporting the notion that the localization of RP-mRNAs to cell protrusions is a universal phenomenon.

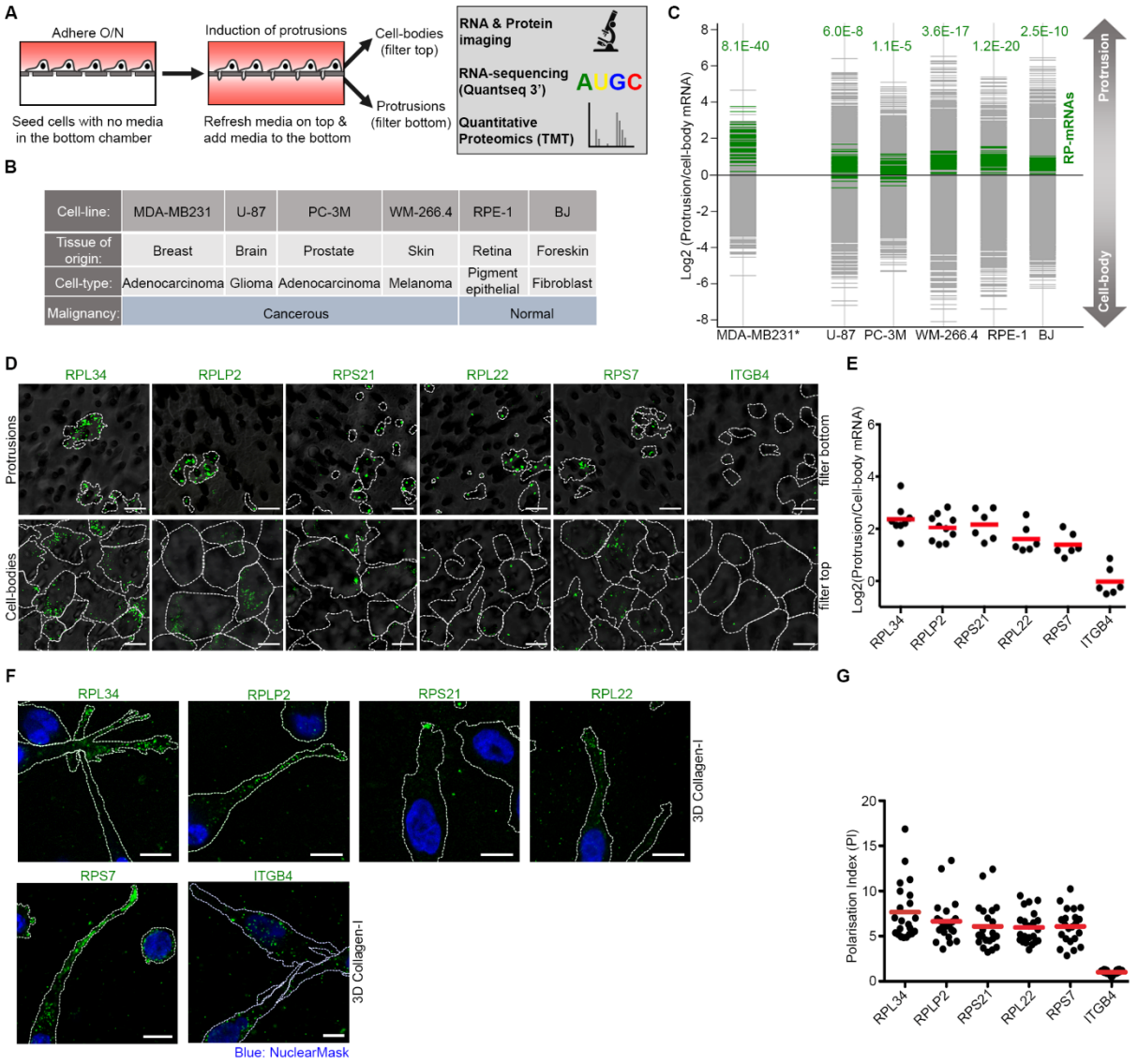

Figure 1: RP-mRNAs universally localize to protrusions. (A) Schematic representation of transwell based protrusion vs. cell-body analysis experiments. **(B)** Panel of normal and malignant cell-lines from diverse tissues of origin, chosen for transwell based profiling. **(C)** RP-mRNAs are ubiquitously enriched in protrusions. Transcriptome distributions between protrusion and cell-body fractions were measured by RNA-sequencing in the panel of cell-lines outlined in (B) (Dataset S1). RP-mRNAs are highlighted in green. Benjamini-Hochberg corrected *P*-values of the RP-mRNA enrichments in protrusions are reported on top of each chart. *MDA- MB231 data was obtained from (Mardakheh et al., 2015) **(D)** Validation of RP-mRNA localization to protrusions by RNA-FISH. Representative RNA-FISH confocal images of protrusions and cell-bodies of MDA-MB231 cells, stained with probes against the indicated RP-mRNAs, or ITG4B mRNA as negative control (Green). Cell boundaries (dashed lines) were defined by co-staining of the cells with anti-tubulin antibody or CellTracker. The filters (grey) were visualized by transmitted light microscopy. **(E)** Quantification of protrusion to cell-body RNA-FISH ratio values from experiments shown in (D). A total of 6-10 field of view images from two biological replicate experiments were quantified per each probe. **(F)** RP-mRNAs localize to the protrusions of MDA-MB231 cells as they invade through 3D collagen-I matrix. Representative RNA-FISH images of MDA-MB231 cells invading through 3D Collagen-I gels as described in Fig. S1D, stained with probes against the indicated RP-mRNAs or ITG4B mRNA as negative control (Green). Cell boundaries (dashed lines) were defined from co-staining with anti-tubulin antibody. **(G)** Quantification of the polarization index (PI) values (Park et al., 2012) for the experiments shown in (F), as a measure of displacement of mRNAs away from the cell-body. Each data point represents the PI value for a single quantified cell. All scale bars are 10 µm. Red dashes on strip charts represent the mean.

Next, we validated our RNA-seq results by RNA-Fluorescence *In Situ* Hybridization (FISH). We used specific RNA-FISH probes against five of the top protrusion enriched RP-mRNAs in the RNA-seq data from MDA-MB231 cells (Dataset S1). All five RP-mRNAs were also found to be enriched in protrusions of MDA-MB231 cells by RNA-FISH (Figure 1D, 1E, & S1A). In contrast, ITGB4 mRNA, which was found to be depleted from protrusions of MDA-MB231 cells by RNA-seq (Dataset S1), did not show an enrichment in protrusions by RNA-FISH (Figure 1D, 1E, & S1A). We then assessed the temporal dynamics of RP-mRNAs localization to protrusions. Time-course induction of protrusions followed by RNA-FISH revealed RP-mRNAs to be enriched from as early as one hour post induction (Figure S1B & S1C). This enrichment was persistent for up to 8 hours (Figure S1B & S1C), suggesting that the localization of RP-mRNAs to protrusions in not a transient phenomenon.

To confirm that the observed enrichment of RP-mRNAs is not restricted to transwell settings, we next assessed the localization of RP-mRNAs in actively migrating MDA-MB231 cells. We chose to assess cell-migration in 3D as it is more relevant to the movement of cells *in vivo* (Sahai, 2005). Moreover, protrusion formation through micro-porous filters is particularly a good mimic for protrusion formation in 3D matrices where cells similarly extend through matrix pores and holes (Mardakheh et al., 2015). RNA-FISH analysis of MDA-MB231 cells invading through a 3D collagen-I matrix (Figure S1D) revealed RP-mRNAs to be highly enriched at the tip of cell-protrusions (Figure 1F, & 1G). In contrast, ITGB4 mRNA remains mostly localized to the perinuclear region within the cell-body (Figure 1F, & 1G). Collectively, these results suggest that RP-mRNAs localization to protrusions is a conserved and persistent feature of mesenchymal-like cells migrating in 3D.

Depletion of LARP proteins reveals a role for LARP6 in RP-mRNAs localization to protrusions

We next set out to determine the molecular mechanism of RP-mRNAs localization to protrusions. Localization of mRNAs is driven by specific RBPs which bind to and mediate transport or subcellular anchoring of their target transcripts (Eliscovich and Singer, 2017). We therefore hypothesized that specific protrusion localized RBPs must be interacting with and localizing RP-mRNAs to protrusions. As RP-mRNAs localization was conserved across all the cell-lines we tested (Figure 1C), such localizing RBPs must also be present in protrusions of all them. To reveal conserved protrusion localized RBPs, we first profiled the distribution of proteins between protrusions and cell-bodies in our panel of cell-lines by tandem mass tagging (TMT) quantitative proteomics (McAlister et al., 2012) (Figure 2A & Dataset S2). We then evaluated which known RBPs were enriched in protrusions of all the cell-lines (Figure 2A). A total of 96 RBPs were identified, several of which belong to structurally/functionally related categories (Figure 2A). These include translation initiation factors, translation elongation factors, Exosome core complex, Cold-Shock Domain (CSD) containing proteins, and the La Related Proteins (LARPs) (Figure 2A). Crucially, the prototypical LARP family member, LARP1, has been previously shown to directly interact with RP-mRNAs through their 5' Terminal Oligo-Pyrimidine (5' TOP) motif, a characteristic stretch of 6-12 pyrimidines at the 5' end of many mRNAs which code for proteins involved in the translation machinery (Fonseca et al., 2015; Lahr et al., 2017; Tcherkezian et al., 2014). This interaction is known to be regulated by the mammalian Target of Rapamycin Complex-1 (mTORC1), ultimately acting to control RP-mRNAs translation and ribosome biogenesis downstream of the mTORC1 pathway (Hong et al., 2017). We therefore assessed whether LARP1 was important for RP-mRNAs localization to protrusions, using an RNA-FISH probe against RPL34 mRNA, which is one of the most enriched RP-mRNAs in protrusions of MDA-MB231 cells (Figure 1D). siRNA mediated depletion of LARP1 did not have an impact on RPL34 mRNA localization to protrusions (Figure

2B & 2C). Accordingly, inhibition of mTORC1 did not affect RPL34 mRNAs localization to protrusions (Figure S2A-C), together suggesting that RP-mRNAs localization must be independent of the mTORC1-LARP1-TOP pathway.

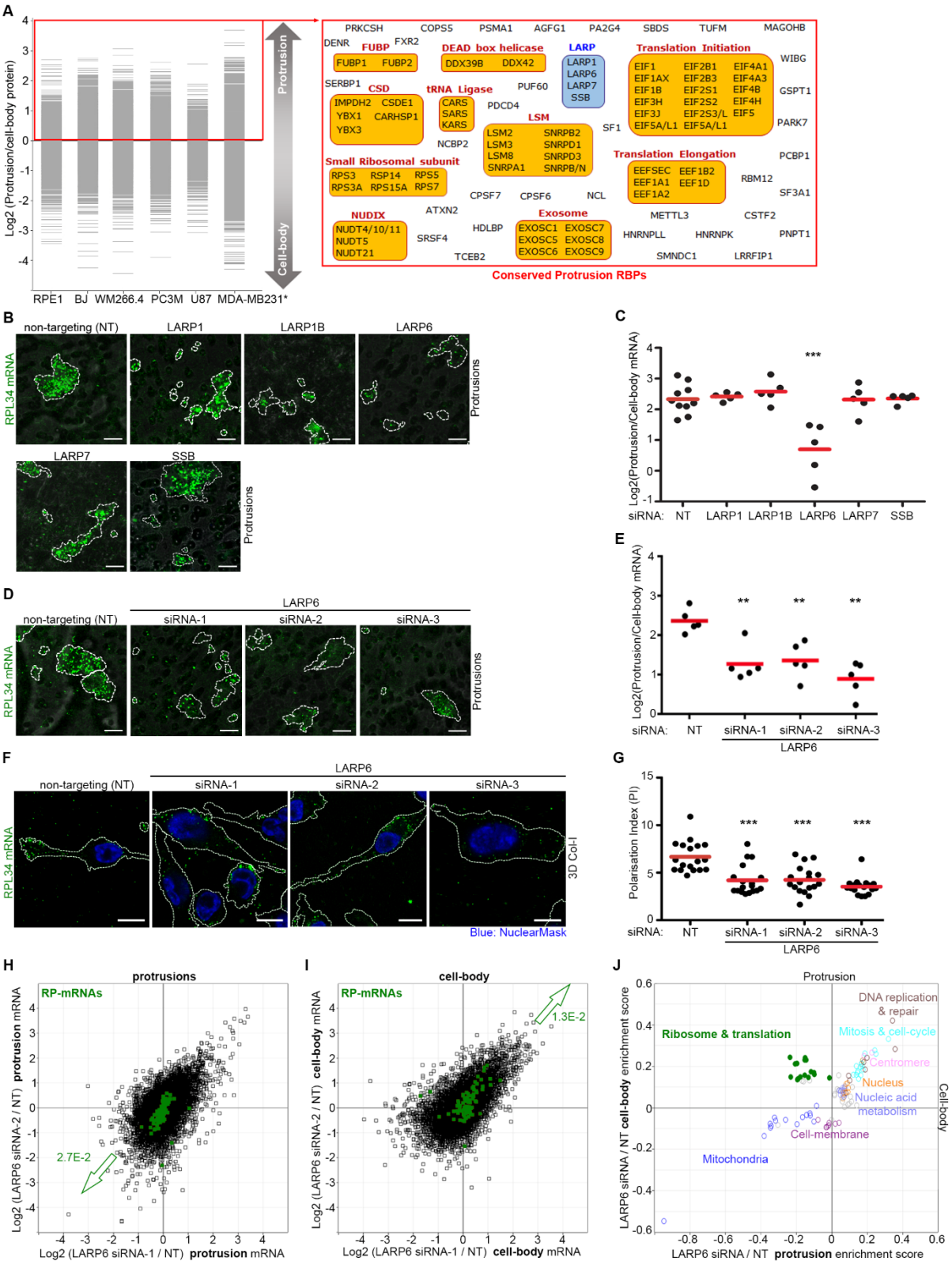

Figure 2: LARP6 localizes RP-mRNAs to protrusions. (A) Quantitative proteomics reveals conserved protrusion-enriched RBPs. Proteome distributions between protrusion and cell-body fractions of the cell-lines listed in Fig. 1B were measured by TMT mediated quantitative proteomics (Dataset S2). Proteins defined as 'RNA-binding'

according to Gene Ontology (GO) Molecular Function database, which were found to be present more in protrusions of all cell-lines, are listed in the red rectangle. RBPs belonging to the same structural/functional families are grouped together. *MDA-MB231 data was obtained from (Mardakheh et al., 2015) **(B)** siRNA screening reveals LARP6 as a crucial regulator of RP-mRNA localization to protrusions. Representative RNA-FISH images of RPL34 mRNA in protrusions of MDA-MB231 cells (green) transfected with non-targeting (NT) control or indicated siRNAs. Cell boundaries (dashed lines) were defined from co-staining with anti-tubulin antibody. The transwell filters (grey) were visualized by transmitted light microscopy. **(C)** Quantification of RPL34 mRNA enrichment in protrusions from experiments shown in (B). Each data-point represents a field of view image, pooled from three biological replicates. *P*-values were calculated using two-tailed homoscedastic t-test. ***$P<0.001$. **(D)** Validation of LARP6 by three independent siRNAs. Representative RNA-FISH images of RPL34 mRNA in protrusions of MDA-MB231 cells (green) transfected with control or three independent LARP6 siRNAs. Cell boundaries (dashed lines) were defined from co-staining with anti-tubulin antibody. The transwell filters (grey) were visualized by transmitted light microscopy. **(E)** Quantification of RPL34 mRNA enrichment in protrusions from experiments shown in (D). Each data-point represents a field of view image, pooled from two independent biological replicates. *P*-values were calculated using two-tailed homoscedastic t-test. **$P<0.01$. **(F)** LARP6 depletion prevents RP-mRNAs localization to protrusions of 3D invading MDA-MB231 cells. Representative RNA-FISH images of RPL34 mRNA distributions in NT or LARP6 siRNA transfected cells (green) invading through 3D Collagen-I matrix, as described in Fig. S1D. Cell boundaries (dashed lines) were defined from co-staining with anti-tubulin antibody. **(G)** Quantification of the polarization index values from experiments shown in (F) as a measure of displacement of mRNAs away from the cell-body. Each data point represents the PI value for a single quantified cell. *P*-values were calculated using two-tailed, homoscedastic t-test. ***$P<0.001$. **(H)** Depletion of LARP6 reduces RP-mRNA levels in protrusions. MDA-MB231 cells transfected with NT control or 2 independent LARP6 siRNAs were subjected to transwell fractionation followed by RNA-sequencing. Log2 of NT/LARP6 KD read counts for all transcripts in protrusions are plotted (Dataset S3), with RP-mRNAs marked in green. Benjamini-Hochberg corrected *P*-value of RP-mRNAs depletion in protrusions is reported on the graph. **(I)** Depletion of LARP6 increases RP-mRNA levels in cell-bodies. Log2 of NT/LARP6 KD read counts for all transcripts in cell-bodies of the cells described in (H) are plotted (Dataset S3), with RP-mRNAs marked in green. Benjamini-Hochberg corrected *P*-value of the RP-mRNA increase in cell-bodies is reported on the graph. **(J)** RP-mRNAs are mis-localized to cell-bodies upon LARP6 depletions. 2D-annotation enrichment analysis of data shown in (H) & (I). Each data point represents a functional category from GO and Kyoto Encyclopedia of Genes and Genomes (KEGG) databases, with similar categories being highlighted in the same colors (Dataset S4). Upon knockdown of LARP6 with two independent siRNAs, mRNAs coding for ribosomal and translation-related categories (green) change in an anti-correlative fashion, suggestive of mis-localization. All other significantly altered categories change in a correlative fashion, suggesting that their levels have changed throughout the cell. All scale bars are 10 µm. Red dashes on strip charts represent the mean.

We next assessed whether any of the other protrusion enriched LARP family members could be important for RP-mRNAs localization. We systematically depleted the LARP family members which were found to be enriched in protrusions of all our cell-lines (Figure 2A), as well as LARP1B which was found as enriched in five out of the six lines but not identified in the remaining (Dataset S2). Only the depletion of LARP6 resulted in a significant decrease in protrusion localization of RPL34 mRNA (Figure 2B & 2C). This decrease was reproduced by three independent siRNAs against LARP6, all of which significantly reduced RPL34 mRNA localization to protrusions (Figure 2D, 2E & S2D). Importantly, depletion of LARP6 did not have an impact on the ability of the cells to form protrusions per se (Figure S2E), suggesting that its effect must be specific to mRNA localization. Localization of RPL34 mRNA to protrusions of 3D invading MDA-MB231 cells was also significantly reduced upon LARP6 depletion (Figure 2F & 2G). Furthermore, CRISPR/Cas9 mediated knockout (KO) of LARP6 similarly resulted in reduced RPL34 mRNA localization to protrusions (Figure S2F-S2H), further confirming that the observed effects of LARP6 loss on RPL34 mRNA localization are not off-target.

To confirm that the impact of LARP6 depletion was not restricted to just one RP-mRNA (i.e. RPL34), we carried out an RNA-seq analysis of protrusion and cell-body fractions from control and LARP6 knockdown cells. Depletion of LARP6 by two independent siRNAs resulted in a significant decrease in levels of RP-mRNAs in the protrusion fraction of MDA-MB231 cells (Figure 2H and Dataset S3). This decrease was concomitant with an increase in the RP-mRNA levels in the cell-body fraction (Figure 2I and Dataset S3), strongly suggesting that LARP6 depletion must be resulting in mis-localization of RP-mRNAs from protrusions to cell-bodies. Accordingly, 2-Dimensional annotation enrichment analysis (Cox and Mann, 2012) revealed RP-mRNA and translation related categories to be specifically regulated in an opposite manner in protrusion and cell-bodies following LARP6 depletion (Figure 2J and Dataset S4). Notably, quantitative proteomics analysis of the protrusion and cell-body fractions following LARP6 depletion showed no significant impact on the subcellular distribution of the proteome (Figure S2I), suggesting that LARP6 depletion does not change the protein composition of protrusions, but affects localization of specific categories of mRNAs.

Transcriptome-wide iCLIP studies reveal direct binding of LARP6 to RP-mRNAs

We next investigated the localization and function of LARP6. To study the subcellular localization of LARP6, we used immunofluorescence (IF) staining with a specific antibody against LARP6 (Figure S3A & S3B). LARP6 was found to be localized to granules which closely track microtubules (Figure 3A). As many RBPs that are involved in RNA localization are known to be associated with the microtubule transport machinery (Bullock, 2011), these results support a role for LARP6 in RNA localization. Furthermore, in agreement with proteomics enrichment of LARP6 in protrusions (Figure S3C), IF analysis revealed LARP6 granules to be highly enriched in protrusions (Figure 3B & 3C). Importantly, a fraction of RPL34 mRNA co-localizes with LARP6 granules, with the co-localization being significantly enhanced in protrusions (Figure 3D & 3E). Given the co-localization of RP-mRNAs with LARP6 granules in protrusions, we wished to determine whether they directly interact. Collagen type I alpha-1 and alpha-2 (COL1A1 & COL1A2) mRNAs have so far been the only known mRNA partners of LARP6 (Cai et al., 2010; Martino et al., 2015). LARP6 was shown to bind a conserved stem loop in the 5'UTR of COL1A1 & COL1A2 mRNAs and stimulate their translation (Blackstock et al., 2014). However, COL1A1 and COL1A2 mRNAs were enriched in the cell-bodies of the many cell lines we examined in our study (Figure S3D), indicating that other mRNA partners are likely to be relevant for the LARP6 function in protrusions. We used MDA-MB231 cells that stably express GFP tagged LARP6 or GFP alone as control (Figure S3E), and exposed them to a short dose of UV-C light to crosslink direct protein-RNA interactions We then performed individual-nucleotide resolution UV crosslinking and immunoprecipitation (iCLIP) (Konig et al., 2010) by purifying the crosslinked LARP6-RNA complexes using anti-GFP beads, and identifying the RNA binding sites of LARP6 across the transcriptome. In agreement with LARP6 cytoplasmic localization (Figure 3A), its crosslinking was strongly enriched on exons compared to introns (Figure S3F). Amongst mRNAs, crosslinking on 3'UTRs was 2-3 fold higher compared to 5'UTR and Open Reading Frame (ORF) sequences (Figure S3F). Analysis of crosslink sites at aligned 5'UTR sequences revealed spikes of LARP6 specific crosslinks at the vicinity of the transcription start site (TSS) (Figure 3F). A clear spike of LARP6 specific crosslinks was also observed at the translation start site (Figure 3G), whilst no apparent positional bias was evident in distribution of LARP6 crosslinks at the 3'UTR (Figure 3H).

Next, we searched for clusters of LARP6 crosslinking across the genome, which identified 18390 peaks corresponding to likely LARP6 binding sites (Dataset S5). These peaks mapped to a total of 5436 genes (Dataset S6), the vast majority of which were protein coding (Figure

3I). Category enrichment analysis revealed RP coding transcripts (i.e. RP-mRNAs) as the most enriched category (Figure 3J & Dataset S7), with LARP6 iCLIP peaks found in 73 out of 80 RP-mRNAs (Dataset S6). Other significantly enriched categories included transcripts involved in RNA processing, intracellular trafficking, cell migration, adhesion, and Extracellular Matrix (ECM), among others (Figure 3J & Dataset S7). Together, these results reveal that LARP6 binds a plethora of transcripts that are important for regulation of cell-proliferation and migration, with RP-mRNAs constituting the most enriched category.

We then investigated the mechanism of LARP6 binding and regulation of RP-mRNAs. Most iCLIP peaks within RP-mRNAs were located in the ORF, with the remaining peaks mainly mapping to the 5'TOP motif, followed by the 3'UTR, and a minor proportion to regions downstream of 5'TOP in the 5'UTR (Figure 3K). Most RP-mRNAs contained multiple LARP6 iCLIP peaks which often mapped to different regions (e.g. ORF and 5'TOP together) (Figure 3L & S3G). We also detected LARP6 peaks within introns of 43 RP genes, but the majority of these peaks fully overlapped with 37 annotated Small nucleolar RNAs (SNORs) that are encoded within the introns of RP genes (Figure 3L & S3G). The positioning of these peaks indicates that LARP6 also binds to SNORs that are processed from the introns of RP-mRNAs.

As the 5'TOP motif is the most characteristic sequence feature within RP-mRNAs, we next investigated whether this motif alone could be sufficient for localizing mRNAs to protrusions. We used an MS2 based live-cell single molecule RNA imaging system (Bertrand et al., 1998) to visualize the subcellular localization of reporter mRNAs that contain either a wild-type (WT) or a mutant (MUT) 5'TOP motif (Gentilella et al., 2017). We engineered MDA-MB231 cells to stably co-express a GFP tagged MS2 Coat Protein (GFP-MCP) with doxycycline inducible WT or MUT 5'TOP mRNA reporters containing the ORF region of β-globin followed by twelve MS2 hairpin repeats in their 3'UTR (Gentilella et al., 2017) (Figure 3M). In the absence of doxycycline, GFP-MCP exhibited a strong nuclear enrichment, which is due to the presence of a Nuclear Localization Signal (NLS) (Bertrand et al., 1998), along with a diffuse cytoplasmic localization pattern (Figure S3H & Movie S1). Upon induction of the WT 5'TOP reporter, GFP-MCP associated with the MS2 repeats, allowing visualization of individual mRNAs molecules as GFP positive cytoplasmic particles (Figure S3H & Movie S2). A similar pattern was observed with the MUT 5'TOP reporter (Figure S3I, Movies S3 & S4), demonstrating that the ability of cells to express the reporter mRNAs is not impacted by the 5'TOP motif. Nevertheless, when cells were allowed to form protrusions through transwell filters, significantly more mRNA molecules could be detected in the protrusions with the WT 5'TOP reporter in comparison to MUT 5'TOP (Figure 3N & 3O, Movies S5 & S6). These results demonstrate that a single 5'TOP motif is sufficient to confer mRNA localization to protrusions.

LARP6 binding to STRAP is critical for its protrusion enrichment and RP-mRNA localization

After revealing the RNA interactome of LARP6, we next set out to investigate its protein-protein interactions, using immunoprecipitation coupled with mass spectrometry (IP-MS). MDA-MB231 cells stably expressing GFP-LARP6 or GFP only as control were subjected to GFP immunoprecipitation, and specifically interacting proteins were revealed by label-free quantification (Hein et al., 2015). A total of 35 proteins were identified as significantly interacting with GFP-LARP6 (Figure 4A & Dataset S8). These included STRAP (also known as UNRIP), a previously known interacting partner of LARP6 (Vukmirovic et al., 2013), several known protrusion enriched RBPs such as IGF2BP2, FXR1, FXR2 (Mardakheh et al., 2015), as well a number of cytoskeleton-associated proteins such as CAPZB, CDC42BPB, and MAP4 (Figure 4A & Dataset S8).

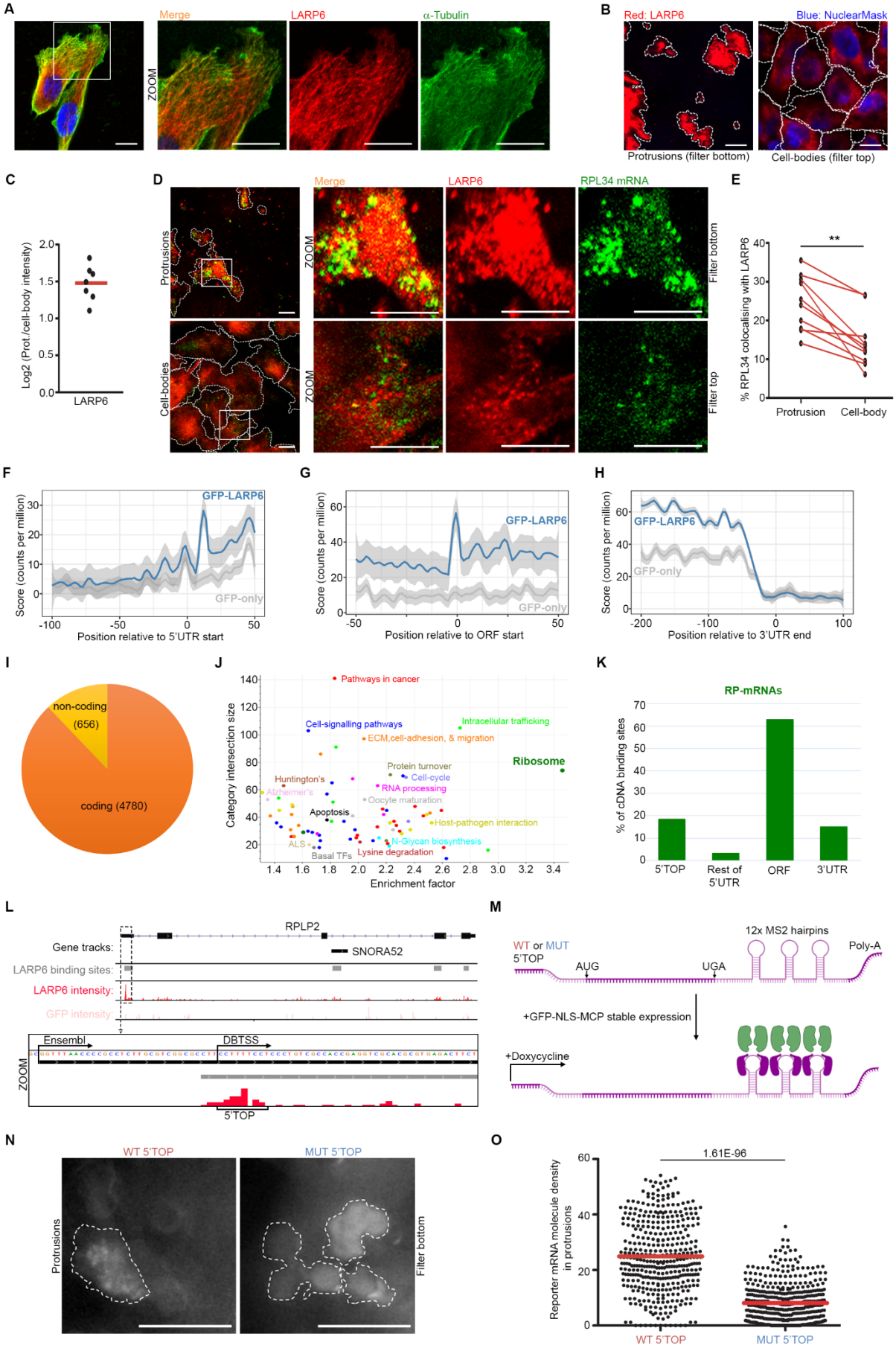

Figure 3: LARP6 is a protrusion enriched RBP which directly binds RP-mRNAs. (A) LARP6 is localized to granules that track the microtubule cytoskeleton. Representative IF images of LARP6 (red) and α-tubulin (green) in MDA-

MB231 cells grown on collagen-coated culture slides. Nucleus was stained with NuclearMask (blue). **(B)** LARP6 granules are enriched in protrusions. Representative IF images of LARP6 (red) in protrusions and cell bodies of MDA-MB231 cells. Cell boundaries (dashed lines) were defined from co-staining with anti-tubulin antibody. **(C)** Quantification of IF images from experiments shown in (B), revealing LARP6 enrichment in protrusions. Log_2 of normalized LARP6 intensities in protrusions/cell bodies from 7 field of view images were quantified. **(D)** LARP6 co-localizes with RP-mRNAs in protrusions. Representative RNA-FISH and IF co-staining images of RPL34 mRNA (green) and LARP6 (red) in protrusions and cell bodies of MDA-MB231 cells. Cell boundaries (dashed lines) were defined from co-staining with anti-tubulin antibody. **(E)** Quantification of the % of co-localization of RPL34 mRNA with LARP6 granules in corresponding protrusion and cell-body images from experiments shown in (D). 10 large field of view images were quantified. Red lines connect values of protrusion and body from same fields of view. *P*-values were calculated using a two-tailed, homoscedastic t-test. ***P*<0.01. **(F)** Metaprofile plot of LARP6 iCLIP crosslink sites at the aligned annotated intergenic-5'UTR junctions (2204 landmarks), showing preferential association with specific regions at the vicinity of TSS. **(G)** Metaprofile plot of LARP6 iCLIP crosslink sites at the aligned annotated 5'UTR-ORF junctions (4122 landmarks), showing preferential association with the translation start site. **(H)** Metaprofile plot of LARP6 iCLIP crosslink sites at the aligned annotated 3'UTR-intergenic junctions (6333 landmarks), showing association throughout the 3'UTR end. **(I)** LARP6 mainly binds protein coding transcripts. Pie chart showing the prevalence of coding vs. non-coding RNAs amongst LARP6 binding targets (Dataset S6). **(J)** The KEGG category of Ribosome (green), which is comprised of RP-mRNAs, is significantly enriched amongst LARP6 binding targets. Fisher's exact test analysis (FDR < 0.02) of mRNA categories which are significantly over-represented amongst the identified LARP6 targets. Each data point represents a functional category from KEGG database, with similar categories being highlighted in similar colors (Dataset S7). **(K)** LARP6 interacts with RP-mRNAs via multiple regions. Distribution of LARP6 binding regions in RP-mRNAs. **(L)** An example genomic view of LARP6 specific binding sites after peak calling (grey) in an RP-mRNA (RPLP2), along with read intensities for GFP-LARP6 and GFP only iCLIP runs. Four distinct LARP6 binding sites are mapped to the RPLP2 locus: two mapping to the ORF region, one to RPLP2 3rd intron which is also annotated as small nucleolar RNA SNORA52, and one to the 5'UTR. Inset: zoomed view of RPLP2 5'UTR showing the LARP6 binding site overlapping with the 5'TOP. Note that for most RP-mRNAs, the Ensembl annotation of TSS is further upstream of the more accurately annotated TSS via TSS-seq in DBTSS (Suzuki et al., 2018). **(M)** Schematic representation of the MS2 reporter system for live cell monitoring of 5'TOP mediated RNA localizations **(N)** WT 5'TOP motif is sufficient for RP-mRNA localization to protrusions. Representative still images of the GFP-MCP signal in transwell protrusions of WT or MUT 5'TOP reporter engineered MDA-MB231 cells described in (M), following induction of reporter expression for 12 hrs with 2μg/ml doxycycline. GFP-MCP exhibits a punctate pattern indicative of association with single mRNA molecules in protrusions of WT 5'TOP reporter expressing cells, but a mostly diffuse pattern in protrusion of MUT 5'TOP reporter expressing cells. **(O)** Quantification of single mRNA molecule counts in protrusions of WT-5'TOP versus MUT-5'TOP reporter expressing cells from experiments shown in (N). A total of 25 (WT) and 28 (MUT) time-lapse videos, each taken for 3 seconds at 0.2 second intervals, were quantified. The number of discrete single-molecule particles identified at every frame image were calculated and normalized to the protrusion area to determine mRNA molecule density in protrusions. The *P*-value was calculated using a two-tailed, homoscedastic t-test. All scale bars are 10 μm. Red dashes on strip charts represent the mean.

We then determined the relative stoichiometry of LARP6 interactors using a computational approach based on intensity-based absolute quantification (iBAQ) (Smits et al., 2013). STRAP was found to be in complex with LARP6 in a super-stoichiometric manner, with every LARP6 molecule being associated with one to two STRAP molecules (Figure 4B). In contrast, all remaining LARP6 interactors were found to be associated with LARP6 in sub-stoichiometric manner (Figure 4B). Accordingly, similar to LARP6, STRAP was found to be enriched in protrusions of all cell types (Figure S4A). As the protein interacting partners of LARP6 included several RBPs (Figure 4A & Dataset S8), we then tested whether the binding of these RBPs, as well as any of the other interactors of LARP6, were mediated indirectly through RNA. Indeed, RNase A treatment of GFP-LARP6 immunoprecipitates resulted in loss of most identified binding partners (Figure 4C & Dataset S9). However, STRAP binding to LARP6 remained unaffected (Figure 4C & Dataset S9), suggesting that it is independent of RNA. Together, these results show that all or most LARP6 molecules are in complex with STRAP through direct

protein-protein interactions, suggesting that STRAP is likely to contribute towards LARP6 function.

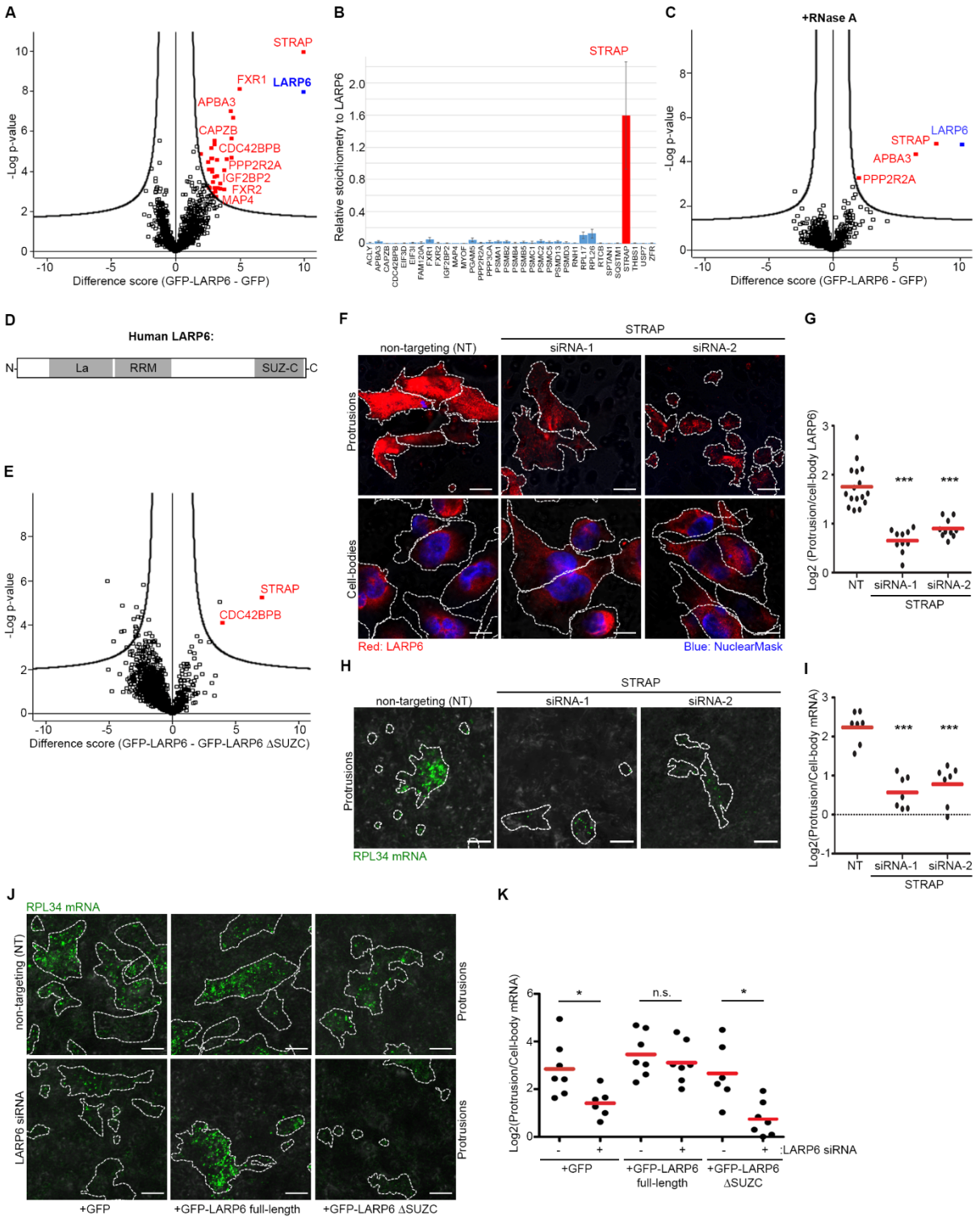

Figure 4: STRAP binding to LARP6 is critical for its protrusion localization and function. (A) LARP6 interacts with STRAP, several protrusion associated RBPs, and a number of cytoskeletal proteins. Volcano plot of GFP-LARP6 versus GFP-only IP-MS data (Dataset S8), with proteins that significantly interact with GFP-LARP6 being marked in red. LARP6 is marked in blue. **(B)** LARP6 binding to STRAP is super-stoichiometric. Analysis of the relative stoichiometry of LARP6-interacting proteins by iBAQ. Average iBAQ values of LARP6-interacting proteins in GFP–LARP6 IPs were subtracted by their corresponding iBAQ values in GFP alone IPs and normalized to the LARP6 iBAQ levels. Error bars are SEM. **(C)** LARP6 binding to STRAP is RNA independent. Volcano plot of RNase A treated GFP-LARP6 versus GFP-only IP-MS data (Dataset S9), with proteins that significantly interact with GFP-LARP6 in

an RNA independent manner being marked in red. LARP6 is marked in blue. **(D)** Schematic diagram of human LARP6 protein domains. La: La motif; RRM: RNA Recognition Motif; SUZ-C: Szy-20 C motif. **(E)** LARP6 binds to STRAP via the SUZ-C domain. Volcano plot of GFP-LARP6 versus GFP-LARP6ΔSUZC IP-MS data (Dataset S10), with previously defined LARP6 interacting proteins that are significantly lost upon SUZ-C deletion being marked in red (Dataset S10). **(F)** STRAP depletion results in loss of LARP6 enrichment in protrusions. Representative IF images of LARP6 (red) in protrusions and cell bodies of MDA-MB231 cells, transfected with NT control or two independent STRAP siRNAs, are shown. Cell boundaries (dashed lines) were defined from co-staining with anti-tubulin antibody. **(G)** Quantification of IF images from experiments shown in (F). Log_2 of normalized LARP6 intensities in protrusions/cell bodies of 6-10 field of view images, pooled from two biological replicate experiments per condition, were quantified. *P*-values were calculated using a two tailed, homoscedastic t-test. ***$P<0.001$. **(H)** Depletion of STRAP inhibits RP-mRNA localization to protrusions. Representative RNA-FISH images of RPL34 mRNA in protrusions of MDA-MB231 cells transfected with NT control or two independent siRNAs against STRAP. Cell boundaries (dashed lines) were defined from co-staining with anti-tubulin antibody. **(I)** Quantification of RPL34 mRNA enrichment in protrusions from experiments shown in (H). Each data-point represents a field of view image pooled from two independent biological replicates. *P*-values were calculated using a two tailed, homoscedastic t-test. ***$P<0.001$. **(J)** Localization of RPL34 mRNA can be rescued by restoring the expression of the full length but not the ΔSUZC mutant LARP6. MDA-MB231 cells stably expressing GFP only, GFP-LARP6, or GFP-LARP6 ΔSUZC were subjected to NT control or a LARP6 siRNA complementary to the 3'UTR region of LARP6, which is absent in GFP-tagged constructs. Representative RNA-FISH images of RPL34 mRNA in protrusions of each condition are shown. **(K)** Quantification of RPL34 mRNA enrichment in protrusions from experiments shown in (J). Each data-point represents a field of view image, pooled from two independent biological replicates. *P*-values were calculated using two-tailed, homoscedastic t -test. *$P<0.05$; n.s.: non-significant. All scale bars are 10 μm. Red dashes on strip charts represent the mean.

Next, we assessed how LARP6 interacts with STRAP. Similar to all LARP family members, LARP6 contains an N-terminal 'La Module' consisted of a La motif followed by an RRM domain, which mediates RNA binding. The C-terminal of the protein, however, differs from other LARP family members as it contains a unique SUZ-C domain that is thought to mediate protein-protein interactions (Stavraka and Blagden, 2015) (Figure 4D). To systematically assess the contribution of each domain towards the protein-protein interactions of LARP6, we generated MDA-MB231 cells stably expressing specific GFP tagged deletion mutants of LARP6 (ΔLa, ΔRRM, and ΔSUZ-C). We then carried out IP-MS as before to quantify changes in the interactome of LARP6 as a result of each deletion. Removal of either La motif or RRM domain did not result in a significant loss of any known interactors (Figure S4B &S4C). However, deletion of the SUZ-C domain significantly reduced LARP6 binding to CDC42BPB and STRAP (Figure 4E & Dataset S10), suggesting that these interactions are mediated via the SUZ-C domain.

In addition to LARP6, STRAP is known to interact with a number of other RBPs such as CSDE1 and multiple SMN complex subunits (Carissimi et al., 2005; Moore et al., 2018). Interaction of the SMN complex with STRAP is known to regulate its subcellular localization (Grimmler et al., 2005). We therefore hypothesized that LARP6 subcellular localization could be similarly regulated by STRAP binding. Indeed, depletion of STRAP with two independent siRNAs resulted in loss of LARP6 enrichment in protrusions (Figure 4F, 4G, & S4D) and a significant decrease in RPL34 mRNA enrichment in protrusions (Figure 4H & 4I). The effect of LARP6 depletion on RPL34 mRNA localization could be rescued by stable expression of an siRNA resistant full-length GFP-LARP6, but not the ΔSUZ-C mutant (Figure 4J & 4K). Together, these results suggest that LARP6 binding to STRAP via its SUZ-C domain is critical for its protrusion localization and enrichment of RP-mRNAs.

LARP6-dependent RP-mRNA localization enhances RP synthesis and ribosome biogenesis

Next, we investigated the functional consequence of RP-mRNA targeting to protrusions via LARP6. Our profiling of protein distributions between protrusions and cell-bodies had revealed many translation initiation and elongation factors as ubiquitously enriched in protrusions (Figure 2A). In fact, time-course analysis of the proteome distribution between protrusions and cell-bodies of MDA-MB231 cells showed that proteins involved in translational initiation and elongation accumulate in protrusions early on (Figure S5A, S5B, and Dataset S11). We therefore hypothesized that this enrichment could lead to higher local levels of translation, making protrusions function as hotspots for protein synthesis in mesenchymal-like cells. To assess this hypothesis, we mapped the subcellular distribution of translation sites in MDA-MB231 cells using RiboPuromycylation (Bastide et al., 2018). In this method, a short pulse of puromycin is administered to the cells along with a translation elongation inhibitor such as Emetine. When administered alone, puromycin gets incorporated into the nascent chain, resulting in premature translation termination and release of the puromycylated peptide (Schmidt et al., 2009). However, in the presence of Emetine, puromycylated peptide remains associated with the stalled ribosome. Subsequent detection of Puromycylated peptides by anti-puromycin antibody results in visualization of the *in situ* translation sites (Bastide et al., 2018). We optimized the RiboPuromycylation method so that it could be used concurrently with RNA-FISH (Figure 5A & S5C), thus allowing the investigation of whether an RNA of interest is associated with translation sites at a given location. In agreement with the observed accumulation of translation initiation and elongation factors in protrusions, time-course RiboPuromycylation analysis of transwell protruding MDA-MB231 cells revealed translation sites to be enriched in protrusions (Figure 5B & 5C). Moreover, concurrent staining with RPL34 mRNA-FISH showed that co-localization of RPL34 mRNA with translation sites was significantly higher in protrusions than the cell bodies (Figure 5B & 5D), suggesting that localization of RP-mRNAs to protrusions likely increases their translation.

Next, we asked whether induction of protrusions increases the synthesis of new RPs. To systematically assess the impact of protrusion formation on translation of RP-mRNAs in the whole cell, we devised a strategy based on pulsed-SILAC (Schwanhausser et al., 2009) (Figure 5E). Light (L) SILAC labelled MDA-MB231 cells were grown overnight on top of two transwell filters. As before, no media was added to the bottom chamber in order to block protrusion formation whilst the cells adhered to the top. The next day, media on top of the filters was changed to Medium (M) or Heavy (H) SILAC media, followed by addition of the same label media to the bottom chamber of one of the transwells in order to open the pores to the cells and allow protrusion formation. Cells were then allowed to form protrusions for 1, 2, 4, or 8 hours, or left without protrusions for the same length of time as control, before lysis of the whole cell (both sides of the filter together) and mixing of differentially pulse-labelled open and closed pore conditions. Following LC-MS/MS analysis, individual H/M SILAC protein ratio values were quantified as measures of relative translation rates between open pore (with protrusions) and closed pore (without protrusions) conditions (Figure 5E). No significant change in translation rates of any protein categories were observed at 1 or 2 hours post protrusion induction (Dataset S12). However, translation of RPs was significantly enhanced after 4 and 8 hours of protrusion induction (Figure 5F & Dataset S12). RPs were in fact the most upregulated category of newly synthesized proteins, followed by a number of RNA processing related categories (Figure S5D & Dataset S13). These results demonstrate that protrusion formation acts to enhance translation of RPs.

Local translation of RP-mRNAs might selectively increase RP abundance just in protrusions. Alternatively, newly made RPs might translocate into the nucleus and nucleolus in order to

interact with maturing rRNAs and thus contribute to ribosome biogenesis (Bohnsack and Bohnsack, 2019). To distinguish between these two possibilities, we combined our pulsed-SILAC strategy with subcellular fractionation of cells into nuclear, membrane, and cytosolic fractions (Figure S5E). Newly synthesized RPs, from both with (open pores) and without (closed pores) protrusion conditions, showed a strong accumulation in the nuclear fraction (Figure S5F & Dataset S14). In contrast, the majority of pre-existing RPs, which constitute RPs in mature ribosomes, were present in the cytosolic fraction (Figure S5G & Dataset S14). These results indicate that similar to the basally translated RPs, most protrusion-synthesized RPs translocate into the nucleus to participate in canonical ribosome biogenesis.

Whilst augmented translation of RP-mRNAs is necessary for increased ribosome biogenesis, newly synthesized RPs are normally degraded if not incorporated into new ribosomes (Lam et al., 2007). We therefore wanted to test whether enhanced translation of RP-mRNAs upon protrusion induction does indeed result in higher stable levels of ribosomal proteins inside the cells. TMT mediated quantitative proteomics comparison of MDA-MB231 cells, with or without protrusions, revealed that whilst short-term (2 hours) induction of protrusions did not significantly change total RP levels, long-term (24 hours) induction resulted in a significant increase in total RP levels (Figure S5H & Dataset S15). Category enrichment analysis revealed that in addition to RPs, other protein categories involved in ribosome biogenesis and rRNA processing, as well as translational regulation (translation initiation, elongation, and termination) were significantly upregulated following protrusion induction (Figure S5I & Dataset S16). In contrast, various mitochondrial and metabolism related categories of proteins showed a significant decrease, suggesting that in addition to upregulation of ribosome biogenesis, a metabolic rewiring program is induced following induction of protrusions (Figure S5I & Dataset S16).

As an increase in ribosome biogenesis ultimately leads to enhancement of the protein synthetic capacity of the cells, we next tested whether induction of protrusions enhanced overall protein synthesis. We assessed overall protein synthesis rates by pulse-labelling with O-propargyl-puromycin (OPP), a click-chemistry variant of puromycin that similarly labels nascent proteins and can be readily visualized by covalent attachment of a fluorescent add-on (Liu et al., 2012). Whilst a short-term (2 hours) induction of protrusions did not result in a change in the OPP labelling levels, long-term (24 hours) induction resulted in a significant increase in OPP labelling, indicative of enhanced overall protein synthesis (Figure 5G & 5H). Thus, in agreement with the increase in ribosome biogenesis, overall protein synthesis is upregulated following long-term induction of protrusions. We next tested whether the observed increase in ribosome biogenesis and overall protein synthesis following protrusion induction is LARP6 dependent. Depletion of LARP6 by two independent siRNAs inhibited upregulation of RP levels following protrusion induction for 24 hrs (Figure 5I & Dataset S17). Category enrichment analysis revealed that while upregulation of RPs and translation regulation categories was LARP6 dependent, changes in other categories of proteins triggered by protrusion induction were not affected by LARP6 depletion (Figure S5J & Dataset S18). These results suggests that unlike other categories of proteins, upregulation of RPs following protrusion induction is specifically regulated by LARP6. Accordingly, enhancement of protein synthesis rates upon protrusion induction was inhibited upon LARP6 depletion (Figure 5J & 5K). Together, these results demonstrate that LARP6-dependent localization of RP-mRNAs promotes their translation, ultimately leading to enhanced ribosome biogenesis and upregulated overall protein synthesis in the whole cell.

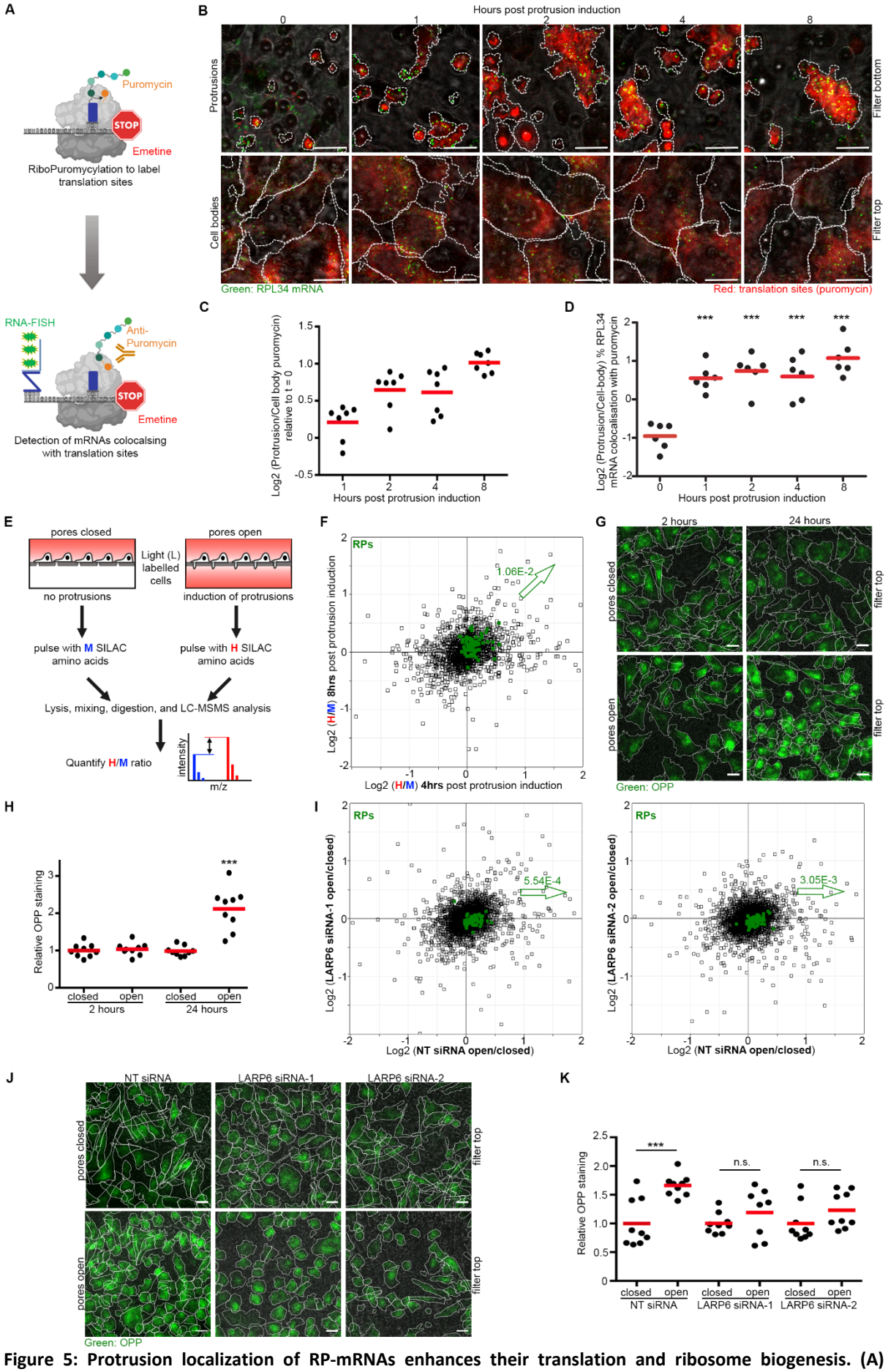

Figure 5: Protrusion localization of RP-mRNAs enhances their translation and ribosome biogenesis. (A) Schematic representation of the Ribopuro-FISH assay. Ribopuromycilation (RPM) coupled with RNA-FISH can be

used to quantify how much an mRNA is associated with active sites of translation. A short pulse of puromycin results in labelling of nascent proteins. When emetine is present, puromycylated peptides remain associated to the ribosome. Detection of these peptides with anti-puromycin antibody visualizes cellular sites of active translation. Co-detection of a specific mRNA by RNA-FISH marks the fraction of mRNA associated with translation sites. **(B)** RP-mRNAs are associated with active sites of translation in protrusions. Representative Ribopuro-FISH images of RPL34 mRNA (green) and puromycin (red) in protrusions and cell bodies of MDA-MB231 cells at the indicated time points post protrusion induction. Cell boundaries (dashed lines) were defined from co-staining with anti-tubulin antibody. All scale bars are 10 µm. **(C)** Translation in protrusions relative to the cell-bodies increases over time. Quantification of puromycin staining intensities in protrusions relative to cell bodies, from experiments shown in (B). A total of 7 field of view images per condition were quantified and normalized to time zero measurements. **(D)** Association of RPL34 mRNAs with active sites of translation is higher in protrusions than cell-bodies. Quantification of % RPL34 mRNA co-localization with puromycin in protrusions relative to cell-bodies from experiments shown (B). A total of 7 field of view images were quantified as in (C). *P*-values were calculated for each time-point relative to time zero, using a two-tailed, homoscedastic t-test. ***$P<0.001$. **(E)** Schematic diagram of pulsed-SILAC proteomics analysis of changes in protein translation rates induced by protrusion formation. H/M, heavy: medium ratios for each protein were determined as measurement of translation rate changes between open pore (cells with protrusions) and closed pore (cells without protrusions) conditions. **(F)** Protrusion formation enhances the translation of RPs. Log2 of H/M ratio values at 4 and 8 hrs post protrusion induction were plotted against each other (Dataset S12). Translation of RPs (green) is significantly increased at both time-points post protrusion induction. Benjamini-Hochberg corrected *P*-value of H/M ratio increase for RPs is reported on the graph. **(G)** Protrusion formation enhances overall protein synthesis. Transwell seeded MDA-MB231 cells were either prevented from protruding through pores (pores closed), or allowed to form protrusions (pores open), for 2 or 24 hrs, before labelling with OPP for 15 mins. OPP was then visualized by Click chemistry mediated addition of Alexa Fluor-488. Representative images of the cells from top of the filters at indicated time points are displayed. NuclearMask blue staining was used to detect individual cells. Scale bars are 20 µm. **(H)** Quantification of OPP staining levels relative to NuclearMask blue. A total of 9 field of view images per condition from experiments shown in (G) were quantified. *P*-values were calculated using two-tailed, homoscedastic t-test. ***$P<0.001$. **(I)** LARP6 depletion blocks protrusion induced enhancement in RP levels. Proteome changes between closed pore and open pore (24 hrs) conditions in NT control vs. LARP6 siRNA treated MDA-MB231 cells were quantified by TMT quantitative proteomics (Dataset S17). Benjamini-Hochberg corrected *P*-values of ratio increase for RPs in NT cells is reported on each graph. **(J)** LARP6 depletion inhibits protrusion induced enhancement of overall protein synthesis. Transwell seeded NT control and LARP6 siRNA treated MDA-MB231 cells were either prevented from protruding through pores (pores closed), or allowed to form protrusions (pores open) for 24 hrs, before labelling with OPP for 15 mins. OPP was then visualized by Click chemistry mediated addition of Alexa Fluor-488. Representative images of the cells from top of the filters are displayed. NuclearMask blue staining was used to detect individual cells. Scale bars are 20 µm. **(K)** Quantification of OPP staining levels relative to NuclearMask blue. A total of 9 field of view images per condition from experiments shown in (J) were quantified. *P*-values were calculated using two-tailed, homoscedastic t-test. n.s.: non-significant; ***$P<0.001$. Red dashes on strip charts represent the mean.

LARP6 is important for ribosome biogenesis in mesenchymal-like cancer cells

We next investigated whether LARP6 contributes toward a significant proportion of RP synthesis in highly migratory mesenchymal-like cancer cells. Using SILAC, we quantified the impact of LARP6 depletion on the proteome of actively growing MDA-MB231 cells (Figure 6A). Levels of RPs were significantly decreased with two independent siRNAs against LARP6 (Figure 6B & Dataset S19). Category enrichment analysis revealed that while the expression of a number protein categories was modulated upon LARP6 depletion, RPs were amongst the most downregulated categories (Figure S6A & Dataset S20). As availability of RPs is crucial for the processing and maturation of rRNAs during ribosome biogenesis, a substantial decrease in their expression results in accumulation of otherwise transient pre-rRNA transcripts which can be detected by RT-qPCR (Pineiro et al., 2018). Accordingly, depletion of LARP6 resulted in a significant accumulation of pre-rRNAs that contain the 5' External Transcribed Spacer (5'ETS) (Figure 6C), suggesting that the decrease in RP levels due to loss of LARP6 must be significant enough to hamper rRNA processing.

Increased ribosome biogenesis underpins various aspects of malignancy such as enhanced proliferation and invasion (Pelletier et al., 2018). Thus, we next assessed whether loss of LARP6 compromised growth and invasion of highly migratory mesenchymal-like cancer cells. siRNA mediated depletion of LARP6 significantly reduced the ability of MDA-MB231 cells to invade through 3D Collagen (Figure 6D & 6E). Knockdown of LARP6 also decreased the viability of MDA-MB231 cells, but this decrease was only significant after longer-term depletion of LARP6 (Figure S6B), suggesting that the observed decrease in invasiveness is unlikely to be due to loss of viability. Accordingly, siRNA depletion of LARP6 significantly affected the long-term growth of MDA-MB231 cells as revealed by clonogenic assays (Figure 6F & 6G). Interestingly, in contrast to siRNA depleted cells, CRISPR/Cas9 KO clones of LARP6 are viable and only mildly, albeit still significantly, affected by loss of LARP6 (Figure S6C). As cells undergo long-term selection during isolation of outgrowing single CRISPR/Cas9 clones, it is possible that other mechanisms of RP synthesis have been positively selected for in KO cells, which compensate for loss of LARP6. Recently described transcriptional compensation mechanisms triggered by CRISPR/Cas9 but not RNAi (El-Brolosy et al., 2019; Ma et al., 2019), may also be at play in this discrepancy.

Enhanced expression of LARP6 in cancer is associated with EMT and can be therapeutically targeted by small molecule inhibitors against LARP6.

Since enhanced ribosome biogenesis is a common feature of most high-grade carcinomas, we wondered whether the LARP6 dependent RP synthesis could be upregulated in certain cancers in order to boost ribosome biogenesis. Mining a published proteomics dataset of protein expression levels in a panel of breast carcinoma cell-lines (Lawrence et al., 2015) revealed LARP6 expression to be mainly detectable in cell-lines belonging to the mesenchymal/low Claudin subtype (Figure S6D). This molecular subtype is closely associated with EMT, and is primarily featured in metaplastic breast carcinomas, a rare but highly invasive form of breast cancer with poor prognosis (Taube et al., 2010). To validate that higher LARP6 protein expression was indeed associated with metaplastic breast cancers, we profiled a panel of human breast tumor tissue samples, composed of both metaplastic and non-metaplastic invasive ductal carcinomas (IDCs), by Immunohistochemistry (IHC). Overall, we detected three major patterns of LARP6 staining in our tumor samples: negative staining, weakly positive staining, or strongly positive staining (Figure 6H). LARP6 strongly positive tumors were significantly enriched amongst the metaplastic carcinomas (Figure 6I). In contrast, weakly positive or negative LARP6 tumors were most commonly non-metaplastic (Figure 6I).

We next investigated whether the expression of LARP6 protein was directly regulated by EMT. *In vitro*, EMT can be induced by long-term treatment of epithelial-like cells with TGFβ1, or by forced expression of transcription factors such as Snail or Twist, which act as master inducers of EMT (Taube et al., 2010). Week-long treatment of epithelial-like breast MCF10AT cells with TGFβ1 induced an irreversible EMT phenotype, characterized by upregulation of mesenchymal markers such as Vimentin (VIM) and ZEB1, along with down-regulation of epithelial markers such as E-Cadherin (CDH1) (Figure 6J). Crucially, LARP6 protein expression was also upregulated following EMT induction by TGFβ1 (Figure 6J). Induction of EMT by overexpression of Twist also enhanced LARP6 expression (Figure 6K). Similarly, induction EMT by overexpression of Snail resulted in upregulation of LARP6 (Figure 6L), together revealing that independent triggers of EMT all induce LARP6 expression.

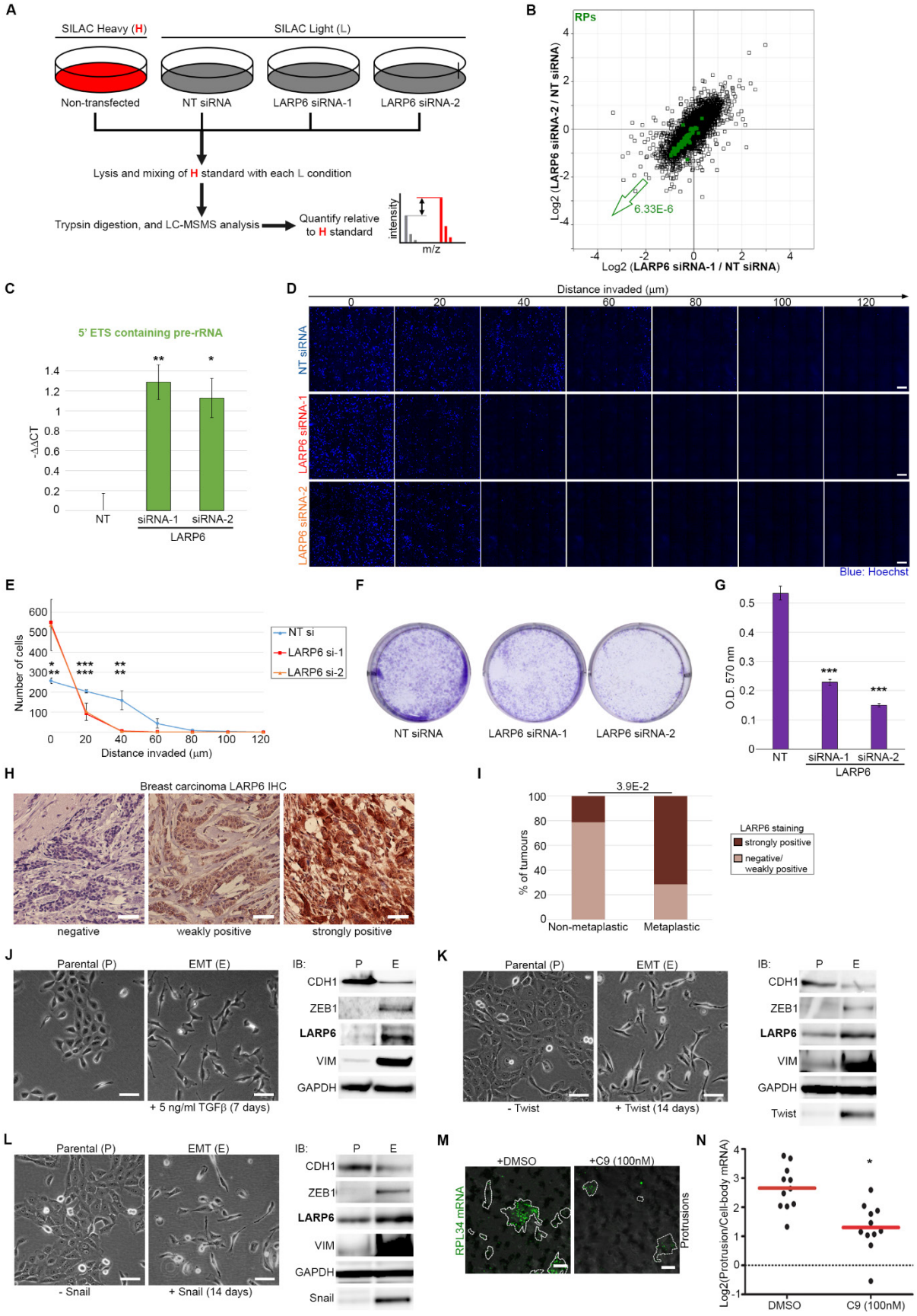

655 **Figure 6: LARP6 is an EMT regulated protein that is necessary for ribosome biogenesis and cell-proliferation in mesenchymal-like cancer cells. (A)** Schematic representation of the proteome analysis of LARP6 depletion by SILAC. Light (L) SILAC labelled MDA-MB231 cells, transfected with NT control or two independent LARP6 siRNAs, were lysed and mixed with Heavy (H) labelled non-transfected MDA-MB231 lysates as reference. H/L ratio values in each mix was then used to calculate relative protein abundance changes between different conditions. **(B)**

LARP6 depletion significantly decreases RP levels in MDA-MB231 cells. Changes in protein levels between MDA-MB231 cells treated with NT control or two independent LARP6 siRNAs for 72 hrs were quantified and plotted (Dataset S19). Benjamini-Hochberg corrected *P*-value of decrease in RP levels is reported on the graph. **(C)** LARP6 depletion results in accumulation of 5'ETS containing pre-rRNAs. RT-qPCR of 5'ETS pre-rRNA in MDA-MB231 cells transfected with NT control or two independent LARP6 siRNAs for 72 hrs. A specific probe against the 5'ETS region, along with a specific probe against GAPDH mRNA as loading control, were used to quantify –ΔΔCT values. Average values were calculated from 2 biological replicates, each performed in 3 technical replicates, per condition. Error bars are SD. *P*-values were calculated using two-tailed, homoscedastic *t*-test. **P*<0.05; ***P*<0.01. **(D)** LARP6 depletion hampers the ability of MDA-MB231 cells to invade through 3D Collagen-I. MDA-MB231 cells were treated with NT control or two independent siRNAs against LARP6 for 72 hrs before being subjected to 3D Collagen-I Invasion assay. 5x5 tiled confocal images of fixed, Hoechst stained cells (blue) at different migrated distances from the start point are displayed. Scale bars are 200 μm. **(E)** Quantification of invaded cell numbers from (D). Average values were calculated from 3-5 biological replicates per condition. Error bars are SD. *P*-values were calculated using two-tailed, homoscedastic *t*-test. **P*<0.05; ***P*<0.01; ****P*<0.001. **(F)** LARP6 depletion decreases growth of MDA-MB231 cells. MDA-MB231 cells were transfected with NT control or two independent LARP6 siRNAs for 72 hrs, before being reseeded to form colonies for a further 10 days prior to crystal violet staining. **(G)** Optical density of crystal violet stained colonies from experiments shown in (F) were measured at 570 nm (OD_{570}) after crystal violet extraction. Average values were calculated from 3 biological replicates each performed in 3 technical replicates. Error bars are SD. *P*-values were calculated using two-tailed, homoscedastic *t*-test. ****P*<0.001. **(H)** Analysis of LARP6 expression in a panel of human breast tumors by IHC. Three distinct patterns of LARP6 expression were detected amongst the tumor samples: 'negative', 'weakly positive', and 'strongly positive'. Representative images for each category are shown. Scale bars are 50 μm. **(I)** LARP6 strongly positive tumors are significantly enriched amongst metaplastic carcinomas. Categorizing tumors based on their LARP6 IHC staining status as in (H) reveals a significant enrichment of LARP6 strongly positive tumors amongst metaplastic carcinomas. The *P*-value was calculated using Fisher's exact test. **(J)** Induction of EMT by human TGFβ1 upregulates LARP6. Left: morphology of MCF10AT cells, following mock treatment or TGFβ1 (5ng/ml) treatment for 7 days, reveals EMT induction. Scale bars are 50 μm. Right: IB analysis of EMT markers (CDH1, ZEB1, VIM) and LARP6, on the cells shown in left. GAPDH was used as loading control. P: Parental; E: EMT. **(K)** Induction of EMT by overexpression of Twist upregulates LARP6. Left: morphology of MCF10AT cells stably harboring a doxycycline inducible Twist construct, with or without doxycycline treatment (1μg/ml) for 14 days, reveals EMT induction following Twist overexpression. Scale bars are 50 μm. Right: IB analysis of EMT markers (CDH1, ZEB1, VIM), Twist, and LARP6, on the cells shown in left. GAPDH was used as loading control. P: Parental; E: EMT. **(L)** Induction of EMT by overexpression of Snail upregulates LARP6. Left: morphology of MCF10AT cells stably harboring a doxycycline inducible Snail construct, with or without doxycycline treatment (1μg/ml) for 14 days, reveals EMT induction following Snail overexpression. Scale bars are 50 μm. Right: IB analysis of EMT transition markers (CDH1, ZEB1, VIM), Snail, and LARP6, on the cells shown in left. GAPDH was used as loading control. P: Parental; E: EMT. **(M)** C9 treatment blocks RP-mRNA localization to protrusions. Representative RNA-FISH images of RPL34 mRNA in protrusions (dashed lines) of vehicle (DMSO) or 100 nM C9 treated MDA-MB231 cells. Cells were allowed to form protrusions for 2 hrs in presence of DMSO or C9. Scale bars are 10 μm. **(N)** Quantification of RPL34 mRNA enrichment in protrusions in DMSO vs. C9 treated cells from experiments shown in (M). A total of 11 field of view images were quantified. Red lines represent the mean. *P*-values were calculated using two-tailed, homoscedastic t-test. **P*<0.05.

Due to the disproportionate upregulation of ribosome biogenesis in most high-grade cancers, there has been a great interest in developing novel strategies that can therapeutically target this pathway in clinic (Pelletier et al., 2018). We hypothesized that in cancers with strong EMT features, inhibiting LARP6 could provide a therapeutic opportunity to more specifically target ribosome biogenesis and inhibit malignant growth. In support of this view, induction of EMT in MCF10AT cells enhanced protein synthesis in a LARP6 dependent manner (Figure S6E & S6F). In addition, whilst the viability of parental epithelial-like MCF10AT cells was only mildly affected by LARP6 depletion, viability was considerably reduced in MCF10AT cells that had undergone EMT (Figure S6G). These results suggest that transformed cells which have

undergone EMT are more dependent on LARP6 for supporting protein synthesis and cell-viability. Importantly, recent work has demonstrated that LARP6 can be targeted by specific small molecule inhibitors designed to interfere with its substrate binding. One such compound, named C9, has been shown to inhibit LARP6 binding to the 5' stem-loop of Collagen-I mRNA at nano-molar (nM) concentrations (Stefanovic et al., 2019). To test whether C9 could similarly inhibit LARP6 function in the context of RP-mRNAs, we tested the effect of C9 treatment on RP-mRNAs localization to protrusions. Similar to the siRNA mediated knockdown of LARP6, short-term (2 hrs) treatment of MDA-MB231 cells with C9 significantly inhibited RPL34 mRNA enrichment in protrusions (Figure 6M & 6N). Unfortunately, long-term treatment of cells with C9 was toxic in a non-specific manner, thus preventing us from assessing its impact on LARP6 dependent regulation of protein synthesis and cell-viability. Nevertheless, these results provide proof-of-concept that LARP6 regulation of RP-mRNAs can be inhibited by small-molecule inhibitors that are designed to target its RNA binding.

Discussion

Mesenchymal-like cell migration is a highly resource intensive cellular process that requires dynamic expression of large quantities of actin cytoskeletal, cell-adhesion, and extracellular matrix proteins, most of which are amongst the most abundant proteins in the proteome of mammalian cells (Schwanhausser et al., 2011). Our results here describes a mechanistic link between protrusion formation, which functions as the main driver of mesenchymal-like cell migration, and regulation of ribosome biogenesis, an essential cellular process that defines the protein synthetic capacity of the cells. We demonstrate that as cells protrude into their surrounding matrix, RP-mRNAs become enriched in protrusions, where they come into contact with the locally enriched translation machinery. This results in up-regulation of RP-mRNA translation. The newly synthesized RPs then travel back to the nucleus where they participate in ribosome biogenesis. Ultimately, LARP6 dependent RP-mRNA localization results in upregulation of ribosome biogenesis, leading to enhancement of overall protein synthesis (Figure 7). We propose that this enhancement acts as a feed-forward mechanism, enabling the cells to then produce large quantities of required proteins to support invasive growth. Importantly, a recent study in mammalian gut epithelial cells also demonstrated that the subcellular localization of RP-mRNAs correlated with their translational output, although the mechanism of this localization was not defined (Moor et al., 2017). Instead of the front-back polarity observed in mesenchymal-like cells, gut epithelial cells exhibit apical-basal polarity with distinct protein and mRNA compositions associated with each part of the polarized cell. RP-mRNAs were shown to be primarily localized to the basal portion of the cells in fasting mice, but upon feeding they translocated to the apical portion where the translation machinery was also enriched, thus leading to enhancement of their translation in an analogous feed-forward mechanism (Moor et al., 2017). It remains to be determined whether LARP6, or another LARP family member, is similarly involved in regulation of RP-mRNAs localization in gut cells. Nevertheless, these studies collectively reveal that post-transcriptional regulation by spatial compartmentalization is a previously unappreciated mechanism in controlling RP-mRNA translation and ribosome biogenesis.

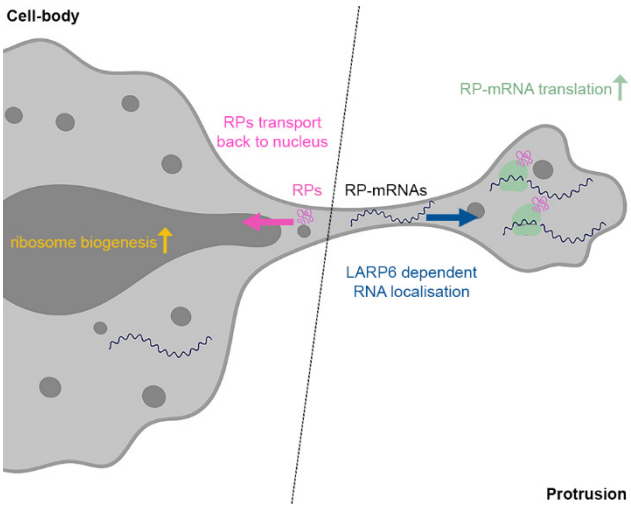

Figure 7: Proposed mechanism of RP synthesis and ribosome biogenesis regulation by LARP6 dependent RP-mRNA localization to cell-protrusions. LARP6 binds RP-mRNAs and localizes them to actin-rich protrusions at the front of migrating mesenchymal-like cells, where their translation is enhanced due to local enrichment of active translation machinery. Once translated, nascent RPs transport back to the nucleus where they participate in ribosome biogenesis, leading to increased ribosome production and augmented overall protein synthesis in actively migrating cells.

Up until now, the mTORC1-LARP1 pathway was the only molecular mechanism known to specifically control the translation of RP-mRNAs (Fonseca et al., 2015; Tcherkezian et al., 2014). LARP1 binds to the 5'cap, 5'TOP, as well as the Poly-A tail of RP-mRNAs (Al-Ashtal et al., 2019), and is thought to be directly phosphorylated on several residues upon activation of mTORC1 (Fonseca et al., 2018). A recent model proposes that these phosphorylation events act as a molecular switch, converting LARP1 from a translational inhibitor to activator, thus upregulating the translation of RP-mRNAs and subsequent ribosome biogenesis (Hong et al., 2017). Our findings here reveal an independent molecular mechanism for translational regulation of RP-mRNAs in synergy with mesenchymal-like cell migration. This suggests that regulation of RP synthesis can be controlled via at least two distinct mechanisms. The interplay between these two pathways under different cellular and environmental conditions remains to be determined.

Hyperactive ribosome biogenesis is a common hallmark as well as a driver of many high-grade cancers (Pelletier et al., 2018; Ruggero and Pandolfi, 2003). It is now evident that various anti-cancer chemotherapies function at least in part by disrupting ribosome biogenesis. Consequently, there has been a surge of interest in identifying more specific ways to target ribosome biogenesis in hope of achieving high anti-tumor activity combined with low genotoxic side effects (Drygin et al., 2011). We here show that LARP6 expression is strongly upregulated by EMT. Moreover, cells which have undergone EMT are more dependent on LARP6 for their protein synthesis and viability, collectively suggesting that LARP6 inhibition could potentially be used as a therapeutic strategy to inhibit ribosome biogenesis in carcinoma subtypes which exhibit a strong EMT signature. In addition to being more invasive, these subtypes often exhibit a greater resistance to standard chemotherapies, collectively resulting in poorer outcome (Dongre and Weinberg, 2019). Importantly, we have shown that a small molecule compound named C9 which interferes with LARP6 RNA binding activity (Stefanovic et al., 2019) can also inhibit RP-mRNA localization to protrusions. Although the safety, efficacy, and pharmacological properties of C9 may not be satisfactory for use in clinic, our results demonstrate the plausibility of therapeutic targeting of LARP6 by small-molecule inhibitors in the context of inhibiting ribosome biogenesis in mesenchymal/EMT associated cancer subtypes.

Experimental procedures

Data availability information, as well as the full list of reagents and detailed experimental procedure are available in supplementary information.

Author contributions

F.K.M. conceived the study and supervised the work. M.Dermit and F.K.M. designed the experiments, interpreted the data, and wrote the manuscript. J.U. and S.P.B. edited the manuscript. M.Dodel generated the CRISPR knockout cell-lines, the MS2 reporter cell-lines, the inducible Twist and Snail cell-lines, and carried out the live cell RNA imaging, as well as the EMT vs. Parental profiling experiments. F.C.Y.L. and M.Dermit carried out the iCLIP experiments and data analysis. J.U. supervised all the iCLIP work. M.S.A performed the Quantseq 3' FWD RNA library preparations. H.S. and S.P.B. validated the C9 compound and determined the effective dose. J.L.J. collected the human breast tumor tissue samples and provided the sections. All other experiments were performed by M.Dermit.

Acknowledgements

We would like to thank C. Gallego, A. Gentilella, A. Yoo, and R. Weinberg for plasmids, and C. Gallego and A. Willis for advice on the experiments. All RNA-seq sequencings were carried out at the Barts and the London Genome Centre. We also wish to acknowledge the role of the Breast Cancer Now Tissue Bank in collecting and making available the human breast tissue samples used in the generation of this publication. Finally, our special thanks goes to C.J. Tape, L. Stojic, T.V. Sharp, and S. McClelland for critical reading of the manuscript. This work was funded by a Medical Research Council Career Development Award (MR/P009417/1) and a Barts Charity grant (MGU0346) to F.K.M.

References

Al-Ashtal, H. A., Rubottom, C. M., Leeper, T. C., and Berman, A. J. (2019). The LARP1 La-Module recognizes both ends of TOP mRNAs. RNA Biol, 1-11.

Andreassi, C., Zimmermann, C., Mitter, R., Fusco, S., De Vita, S., Saiardi, A., and Riccio, A. (2010). An NGF-responsive element targets myo-inositol monophosphatase-1 mRNA to sympathetic neuron axons. Nat Neurosci *13*, 291-301.

Bastide, A., Yewdell, J. W., and David, A. (2018). The RiboPuromycylation Method (RPM): an Immunofluorescence Technique to Map Translation Sites at the Sub-cellular Level. Bio Protoc *8*.

Benoit Bouvrette, L. P., Cody, N. A. L., Bergalet, J., Lefebvre, F. A., Diot, C., Wang, X., Blanchette, M., and Lecuyer, E. (2018). CeFra-seq reveals broad asymmetric mRNA and noncoding RNA distribution profiles in Drosophila and human cells. RNA *24*, 98-113.

Bertrand, E., Chartrand, P., Schaefer, M., Shenoy, S. M., Singer, R. H., and Long, R. M. (1998). Localization of ASH1 mRNA particles in living yeast. Molecular cell *2*, 437-445.

Blackstock, C. D., Higashi, Y., Sukhanov, S., Shai, S. Y., Stefanovic, B., Tabony, A. M., Yoshida, T., and Delafontaine, P. (2014). Insulin-like growth factor-1 increases synthesis of collagen type I via induction of the mRNA-binding protein LARP6 expression and binding to the 5' stem-loop of COL1a1 and COL1a2 mRNA. J Biol Chem *289*, 7264-7274.

Bohnsack, K. E., and Bohnsack, M. T. (2019). Uncovering the assembly pathway of human ribosomes and its emerging links to disease. The EMBO journal *38*, e100278.

Briese, M., Saal, L., Appenzeller, S., Moradi, M., Baluapuri, A., and Sendtner, M. (2016). Whole transcriptome profiling reveals the RNA content of motor axons. Nucleic acids research *44*, e33.

Bullock, S. L. (2011). Messengers, motors and mysteries: sorting of eukaryotic mRNAs by cytoskeletal transport. Biochem Soc Trans *39*, 1161-1165.

Cai, L., Fritz, D., Stefanovic, L., and Stefanovic, B. (2010). Binding of LARP6 to the conserved 5' stem-loop regulates translation of mRNAs encoding type I collagen. J Mol Biol *395*, 309-326.

Carissimi, C., Baccon, J., Straccia, M., Chiarella, P., Maiolica, A., Sawyer, A., Rappsilber, J., and Pellizzoni, L. (2005). Unrip is a component of SMN complexes active in snRNP assembly. FEBS letters *579*, 2348-2354.

Cox, J., and Mann, M. (2012). 1D and 2D annotation enrichment: a statistical method integrating quantitative proteomics with complementary high-throughput data. BMC Bioinformatics *13 Suppl 16*, S12.

Dongre, A., and Weinberg, R. A. (2019). New insights into the mechanisms of epithelial-mesenchymal transition and implications for cancer. Nature reviews Molecular cell biology *20*, 69-84.

Drygin, D., Lin, A., Bliesath, J., Ho, C. B., O'Brien, S. E., Proffitt, C., Omori, M., Haddach, M., Schwaebe, M. K., Siddiqui-Jain, A.*, et al.* (2011). Targeting RNA polymerase I with an oral small molecule CX-5461 inhibits ribosomal RNA synthesis and solid tumor growth. Cancer research *71*, 1418-1430.

El-Brolosy, M. A., Kontarakis, Z., Rossi, A., Kuenne, C., Gunther, S., Fukuda, N., Kikhi, K., Boezio, G. L. M., Takacs, C. M., Lai, S. L.*, et al.* (2019). Genetic compensation triggered by mutant mRNA degradation. Nature *568*, 193-197.

Eliscovich, C., and Singer, R. H. (2017). RNP transport in cell biology: the long and winding road. Curr Opin Cell Biol *45*, 38-46.

Fonseca, B. D., Jia, J.-J., Hollensen, A. K., Pointet, R., Hoang, H.-D., Niklaus, M. R., Pena, I. A., Lahr, R. M., Smith, E. M., Hearnden, J.*, et al.* (2018). LARP1 is a major phosphorylation substrate of mTORC1. bioRxiv, 491274.

Fonseca, B. D., Zakaria, C., Jia, J. J., Graber, T. E., Svitkin, Y., Tahmasebi, S., Healy, D., Hoang, H. D., Jensen, J. M., Diao, I. T.*, et al.* (2015). La-related Protein 1 (LARP1) Represses Terminal Oligopyrimidine (TOP) mRNA Translation Downstream of mTOR Complex 1 (mTORC1). J Biol Chem *290*, 15996-16020.

Gentilella, A., Moron-Duran, F. D., Fuentes, P., Zweig-Rocha, G., Riano-Canalias, F., Pelletier, J., Ruiz, M., Turon, G., Castano, J., Tauler, A.*, et al.* (2017). Autogenous Control of 5'TOP mRNA Stability by 40S Ribosomes. Molecular cell *67*, 55-70 e54.

Granneman, S., and Tollervey, D. (2007). Building ribosomes: even more expensive than expected? Current biology : CB *17*, R415-417.

Grimmler, M., Otter, S., Peter, C., Muller, F., Chari, A., and Fischer, U. (2005). Unrip, a factor implicated in cap-independent translation, associates with the cytosolic SMN complex and influences its intracellular localization. Hum Mol Genet *14*, 3099-3111.

Gumy, L. F., Yeo, G. S., Tung, Y. C., Zivraj, K. H., Willis, D., Coppola, G., Lam, B. Y., Twiss, J. L., Holt, C. E., and Fawcett, J. W. (2011). Transcriptome analysis of embryonic and adult sensory axons reveals changes in mRNA repertoire localization. RNA *17*, 85-98.

Hein, M. Y., Hubner, N. C., Poser, I., Cox, J., Nagaraj, N., Toyoda, Y., Gak, I. A., Weisswange, I., Mansfeld, J., Buchholz, F.*, et al.* (2015). A human interactome in three quantitative dimensions organized by stoichiometries and abundances. Cell *163*, 712-723.

Hong, S., Freeberg, M. A., Han, T., Kamath, A., Yao, Y., Fukuda, T., Suzuki, T., Kim, J. K., and Inoki, K. (2017). LARP1 functions as a molecular switch for mTORC1-mediated translation of an essential class of mRNAs. Elife *6*.

Hsieh, A. C., Liu, Y., Edlind, M. P., Ingolia, N. T., Janes, M. R., Sher, A., Shi, E. Y., Stumpf, C. R., Christensen, C., Bonham, M. J.*, et al.* (2012). The translational landscape of mTOR signalling steers cancer initiation and metastasis. Nature *485*, 55-61.

Kejiou, N. S., and Palazzo, A. F. (2017). mRNA localization as a rheostat to regulate subcellular gene expression. Wiley interdisciplinary reviews RNA *8*.

Lahr, R. M., Fonseca, B. D., Ciotti, G. E., Al-Ashtal, H. A., Jia, J. J., Niklaus, M. R., Blagden, S. P., Alain, T., and Berman, A. J. (2017). La-related protein 1 (LARP1) binds the mRNA cap, blocking eIF4F assembly on TOP mRNAs. Elife *6*.

Lam, Y. W., Lamond, A. I., Mann, M., and Andersen, J. S. (2007). Analysis of nucleolar protein dynamics reveals the nuclear degradation of ribosomal proteins. Current biology : CB *17*, 749-760.

Lawrence, R. T., Perez, E. M., Hernandez, D., Miller, C. P., Haas, K. M., Irie, H. Y., Lee, S. I., Blau, C. A., and Villen, J. (2015). The proteomic landscape of triple-negative breast cancer. Cell reports *11*, 630-644.

Lecuyer, E., Yoshida, H., Parthasarathy, N., Alm, C., Babak, T., Cerovina, T., Hughes, T. R., Tomancak, P., and Krause, H. M. (2007). Global analysis of mRNA localization reveals a prominent role in organizing cellular architecture and function. Cell *131*, 174-187.

Liu, J., Xu, Y., Stoleru, D., and Salic, A. (2012). Imaging protein synthesis in cells and tissues with an alkyne analog of puromycin. Proceedings of the National Academy of Sciences of the United States of America *109*, 413-418.

Ma, Z., Zhu, P., Shi, H., Guo, L., Zhang, Q., Chen, Y., Chen, S., Zhang, Z., Peng, J., and Chen, J. (2019). PTC-bearing mRNA elicits a genetic compensation response via Upf3a and COMPASS components. Nature *568*, 259-263.

Mardakheh, F. K., Paul, A., Kumper, S., Sadok, A., Paterson, H., McCarthy, A., Yuan, Y., and Marshall, C. J. (2015). Global Analysis of mRNA, Translation, and Protein Localization: Local Translation Is a Key Regulator of Cell Protrusions. Developmental cell *35*, 344-357.

Martino, L., Pennell, S., Kelly, G., Busi, B., Brown, P., Atkinson, R. A., Salisbury, N. J., Ooi, Z. H., See, K. W., Smerdon, S. J.*, et al.* (2015). Synergic interplay of the La motif, RRM1 and the interdomain linker of LARP6 in the recognition of collagen mRNA expands the RNA binding repertoire of the La module. Nucleic acids research *43*, 645-660.

McAlister, G. C., Huttlin, E. L., Haas, W., Ting, L., Jedrychowski, M. P., Rogers, J. C., Kuhn, K., Pike, I., Grothe, R. A., Blethrow, J. D., and Gygi, S. P. (2012). Increasing the multiplexing capacity of TMTs using reporter ion isotopologues with isobaric masses. Analytical chemistry *84*, 7469-7478.

Mendillo, M. L., Santagata, S., Koeva, M., Bell, G. W., Hu, R., Tamimi, R. M., Fraenkel, E., Ince, T. A., Whitesell, L., and Lindquist, S. (2012). HSF1 drives a transcriptional program distinct from heat shock to support highly malignant human cancers. Cell *150*, 549-562.

Mili, S., Moissoglu, K., and Macara, I. G. (2008). Genome-wide screen reveals APC-associated RNAs enriched in cell protrusions. Nature *453*, 115-119.

Moor, A. E., Golan, M., Massasa, E. E., Lemze, D., Weizman, T., Shenhav, R., Baydatch, S., Mizrahi, O., Winkler, R., Golani, O.*, et al.* (2017). Global mRNA polarization regulates translation efficiency in the intestinal epithelium. Science *357*, 1299-1303.

Moore, K. S., Yagci, N., van Alphen, F., Meijer, A. B., t Hoen, P. A. C., and von Lindern, M. (2018). Strap associates with Csde1 and affects expression of select Csde1-bound transcripts. PLoS One *13*, e0201690.

Park, H. Y., Trcek, T., Wells, A. L., Chao, J. A., and Singer, R. H. (2012). An unbiased analysis method to quantify mRNA localization reveals its correlation with cell motility. Cell reports *1*, 179-184.

Pelletier, J., Thomas, G., and Volarevic, S. (2018). Ribosome biogenesis in cancer: new players and therapeutic avenues. Nat Rev Cancer *18*, 51-63.

Pineiro, D., Stoneley, M., Ramakrishna, M., Alexandrova, J., Dezi, V., Juke-Jones, R., Lilley, K. S., Cain, K., and Willis, A. E. (2018). Identification of the RNA polymerase I-RNA interactome. Nucleic acids research *46*, 11002-11013.

Pizzinga, M., Bates, C., Lui, J., Forte, G., Morales-Polanco, F., Linney, E., Knotkova, B., Wilson, B., Solari, C. A., Berchowitz, L. E.*, et al.* (2019). Translation factor mRNA granules direct protein synthetic capacity to regions of polarized growth. The Journal of cell biology *218*, 1564-1581.

Prasanth, K. V., Prasanth, S. G., Xuan, Z., Hearn, S., Freier, S. M., Bennett, C. F., Zhang, M. Q., and Spector, D. L. (2005). Regulating gene expression through RNA nuclear retention. Cell *123*, 249-263.

Ruggero, D., and Pandolfi, P. P. (2003). Does the ribosome translate cancer? Nat Rev Cancer *3*, 179-192.

Saal, L., Briese, M., Kneitz, S., Glinka, M., and Sendtner, M. (2014). Subcellular transcriptome alterations in a cell culture model of spinal muscular atrophy point to widespread defects in axonal growth and presynaptic differentiation. RNA *20*, 1789-1802.

Sahai, E. (2005). Mechanisms of cancer cell invasion. Current opinion in genetics & development *15*, 87-96.

Schmidt, E. K., Clavarino, G., Ceppi, M., and Pierre, P. (2009). SUnSET, a nonradioactive method to monitor protein synthesis. Nat Methods *6*, 275-277.

Schwanhausser, B., Busse, D., Li, N., Dittmar, G., Schuchhardt, J., Wolf, J., Chen, W., and Selbach, M. (2011). Global quantification of mammalian gene expression control. Nature *473*, 337-342.

Schwanhausser, B., Gossen, M., Dittmar, G., and Selbach, M. (2009). Global analysis of cellular protein translation by pulsed SILAC. Proteomics *9*, 205-209.

Shigeoka, T., Jung, H., Jung, J., Turner-Bridger, B., Ohk, J., Lin, J. Q., Amieux, P. S., and Holt, C. E. (2016). Dynamic Axonal Translation in Developing and Mature Visual Circuits. Cell *166*, 181-192.

Smits, A. H., Jansen, P. W., Poser, I., Hyman, A. A., and Vermeulen, M. (2013). Stoichiometry of chromatin-associated protein complexes revealed by label-free quantitative mass spectrometry-based proteomics. Nucleic acids research *41*, e28.

Stavraka, C., and Blagden, S. (2015). The La-Related Proteins, a Family with Connections to Cancer. Biomolecules *5*, 2701-2722.

Stefanovic, B., Manojlovic, Z., Vied, C., Badger, C. D., and Stefanovic, L. (2019). Discovery and evaluation of inhibitor of LARP6 as specific antifibrotic compound. Sci Rep *9*, 326.

Suzuki, A., Kawano, S., Mitsuyama, T., Suyama, M., Kanai, Y., Shirahige, K., Sasaki, H., Tokunaga, K., Tsuchihara, K., Sugano, S.*, et al.* (2018). DBTSS/DBKERO for integrated analysis of transcriptional regulation. Nucleic acids research *46*, D229-D238.

Taube, J. H., Herschkowitz, J. I., Komurov, K., Zhou, A. Y., Gupta, S., Yang, J., Hartwell, K., Onder, T. T., Gupta, P. B., Evans, K. W.*, et al.* (2010). Core epithelial-to-mesenchymal transition interactome gene-expression signature is associated with claudin-low and metaplastic breast cancer subtypes. Proceedings of the National Academy of Sciences of the United States of America *107*, 15449-15454.

Taylor, A. M., Berchtold, N. C., Perreau, V. M., Tu, C. H., Li Jeon, N., and Cotman, C. W. (2009). Axonal mRNA in uninjured and regenerating cortical mammalian axons. J Neurosci *29*, 4697-4707.

Tcherkezian, J., Cargnello, M., Romeo, Y., Huttlin, E. L., Lavoie, G., Gygi, S. P., and Roux, P. P. (2014). Proteomic analysis of cap-dependent translation identifies LARP1 as a key regulator of 5'TOP mRNA translation. Genes Dev *28*, 357-371.

Thoreen, C. C., Chantranupong, L., Keys, H. R., Wang, T., Gray, N. S., and Sabatini, D. M. (2012). A unifying model for mTORC1-mediated regulation of mRNA translation. Nature *485*, 109-113.

Vukmirovic, M., Manojlovic, Z., and Stefanovic, B. (2013). Serine-threonine kinase receptor-associated protein (STRAP) regulates translation of type I collagen mRNAs. Molecular and cellular biology *33*, 3893-3906.

Wang, E. T., Cody, N. A., Jog, S., Biancolella, M., Wang, T. T., Treacy, D. J., Luo, S., Schroth, G. P., Housman, D. E., Reddy, S.*, et al.* (2012). Transcriptome-wide regulation of pre-mRNA splicing and mRNA localization by muscleblind proteins. Cell *150*, 710-724.

Wang, T., Hamilla, S., Cam, M., Aranda-Espinoza, H., and Mili, S. (2017). Extracellular matrix stiffness and cell contractility control RNA localization to promote cell migration. Nat Commun *8*, 896.

Wilk, R., Hu, J., Blotsky, D., and Krause, H. M. (2016). Diverse and pervasive subcellular distributions for both coding and long noncoding RNAs. Genes Dev *30*, 594-609.

Zappulo, A., van den Bruck, D., Ciolli Mattioli, C., Franke, V., Imami, K., McShane, E., Moreno-Estelles, M., Calviello, L., Filipchyk, A., Peguero-Sanchez, E.*, et al.* (2017). RNA localization is a key determinant of neurite-enriched proteome. Nat Commun *8*, 583.

Zivraj, K. H., Tung, Y. C., Piper, M., Gumy, L., Fawcett, J. W., Yeo, G. S., and Holt, C. E. (2010). Subcellular profiling reveals distinct and developmentally regulated repertoire of growth cone mRNAs. J Neurosci *30*, 15464-15478.